scientific reports

Check for updates

OPEN

In vivo transomic analyses of glucose-responsive metabolism in skeletal muscle reveal core differences between the healthy and obese states

Toshiya Kokaji[1,2,16], Miki Eto[1,16], Atsushi Hatano[1,3,4], Katsuyuki Yugi[1,3,5,6], Keigo Morita[1], Satoshi Ohno[1,7], Masashi Fujii[1,7,8], Ken-ichi Hironaka[1], Yuki Ito[9,10], Riku Egami[9], Saori Uematsu[9], Akira Terakawa[1], Yifei Pan[9], Hideki Maehara[1], Dongzi Li[1], Yunfan Bai[9], Takaho Tsuchiya[11,12], Haruka Ozaki[11,12], Hiroshi Inoue[13], Hiroyuki Kubota[10], Yutaka Suzuki[9], Akiyoshi Hirayama[14], Tomoyoshi Soga[14] & Shinya Kuroda[1,9,15]✉

Metabolic regulation in skeletal muscle is essential for blood glucose homeostasis. Obesity causes insulin resistance in skeletal muscle, leading to hyperglycemia and type 2 diabetes. In this study, we performed multiomic analysis of the skeletal muscle of wild-type (WT) and leptin-deficient obese (*ob/ob*) mice, and constructed regulatory transomic networks for metabolism after oral glucose administration. Our network revealed that metabolic regulation by glucose-responsive metabolites had a major effect on WT mice, especially carbohydrate metabolic pathways. By contrast, in *ob/ob* mice, much of the metabolic regulation by glucose-responsive metabolites was lost and metabolic regulation by glucose-responsive genes was largely increased, especially in carbohydrate and lipid metabolic pathways. We present some characteristic metabolic regulatory pathways found in central carbon, branched amino acids, and ketone body metabolism. Our transomic analysis will provide insights into how skeletal muscle responds to changes in blood glucose and how it fails to respond in obesity.

[1]Department of Biological Sciences, Graduate School of Science, University of Tokyo, 7-3-1 Hongo, Bunkyo-ku, Tokyo 113-0033, Japan. [2]Data Science Center, Nara Institute of Science and Technology, 8916-5 Takayama, Ikoma, Nara, Japan. [3]Laboratory for Integrated Cellular Systems, RIKEN Center for Integrative Medical Sciences, 1-7-22 Suehiro-cho, Tsurumi-ku, Yokohama, Kanagawa 230-0045, Japan. [4]Department of Omics and Systems Biology, Niigata University Graduate School of Medical and Dental Sciences, 757 Ichibancho, Asahimachi-dori, Chuo-ku, Niigata City 951-8510, Japan. [5]Institute for Advanced Biosciences, Keio University, Fujisawa 252-8520, Japan. [6]PRESTO, Japan Science and Technology Agency, 1-7-22 Suehiro-cho, Tsurumi-ku, Yokohama, Kanagawa 230-0045, Japan. [7]Molecular Genetics Research Laboratory, Graduate School of Science, University of Tokyo, 7-3-1 Hongo, Bunkyo-ku, Tokyo 113-0033, Japan. [8]Department of Mathematical and Life Sciences, Graduate School of Integrated Sciences for Life, Hiroshima University, 1-3-1 Kagamiyama, Higashi-hiroshima City, Hiroshima 739-8526, Japan. [9]Department of Computational Biology and Medical Sciences, Graduate School of Frontier Sciences, University of Tokyo, 5-1-5 Kashiwanoha, Kashiwa, Chiba 277-8562, Japan. [10]Division of Integrated Omics, Medical Research Center for High Depth Omics, Medical Institute of Bioregulation, Kyushu University, 3-1-1 Maidashi, Higashi-ku, Fukuoka 812-8582, Japan. [11]Bioinformatics Laboratory, Faculty of Medicine, University of Tsukuba, Ibaraki 305-8575, Japan. [12]Center for Artificial Intelligence Research, University of Tsukuba, Ibaraki 305-8577, Japan. [13]Metabolism and Nutrition Research Unit, Institute for Frontier Science Initiative, Kanazawa University, 13-1 Takaramachi, Kanazawa, Ishikawa 920-8641, Japan. [14]Institute for Advanced Biosciences, Keio University, 246-2 Mizukami, Kakuganji, Tsuruoka, Yamagata 997-0052, Japan. [15]Core Research for Evolutional Science and Technology (CREST), Japan Science and Technology Agency, Bunkyo-ku, Tokyo 113-0033, Japan. [16]These authors contributed equally: Toshiya Kokaji and Miki Eto. ✉email: skuroda@bs.s.u-tokyo.ac.jp

Blood glucose level is regulated by the cooperative function of many tissues. Insulin, the hormone for lowering blood glucose level, is secreted by pancreatic beta cells when blood glucose level rises. Insulin lowers blood glucose level by stimulating glucose disposal in the skeletal muscle and adipose tissue, and inhibits gluconeogenesis in the liver[1]. Type 2 diabetes mellitus (T2DM) is one of the most devastating results of obesity, and is characterized by insulin resistance and hyperglycemia[2]. Reduced responsiveness of skeletal muscle to insulin is one of the critical aspects of T2DM development[3]. T2DM is a multifactorial disease involving many complex signaling pathways in different tissues; thus, a comprehensive analysis might help further our understanding of the molecular mechanisms of this disease.

Metabolism is a series of chemical reactions that convert starting materials into molecules that maintain the living state of cells and organisms. Metabolic reactions, defined as chemical reactions of metabolism, are regulated by metabolic enzymes and metabolites. Metabolic enzymes mainly regulate metabolic reactions at the gene expression level, which is determined by transcription factors; and at the enzyme activity level, which is regulated by post-translational modifications such as phosphorylation. Metabolites regulate metabolic reactions through the concentration of substrates, and also through the allosteric regulation of enzyme activity.

Integrating multiple omics techniques such as metabolomics, proteomics, and transcriptomics is useful for understanding the flow of biological information, and has been applied to a wide range of biological problems[4,5]. Several groups have used multiomic approaches to study the molecular mechanisms of insulin resistance. One study integrated epigenomics, transcriptomics, proteomics, and metabolomics to analyze the liver of mice fed a high-fat diet[6]. Another study used transcriptomics, proteomics, metabolomics, and microbiomics to analyze blood and stool samples from healthy human participants during weight gain and weight loss[7]. A transomic approach, proposed by our group, connects measurements of multiple omics layers such as proteomics, transcriptomics, and metabolomics based on direct molecular interactions[8–11]. This approach provides an understanding of the spatiotemporal dynamics of the biochemical network.

Because blood glucose homeostasis is achieved by regulating glucose metabolism in the metabolic organs and glucose metabolism is closely related to various metabolisms, the metabolic regulation after glucose intake and the effect of its dysregulation in obesity is considered to be extensive. Indeed, our previous transomic analysis in mouse liver revealed that the metabolic regulatory networks of wild-type and genetically obese mice are globally distinct[12,13]. However, the metabolic regulatory network in muscle, an important organ for glucose metabolism, has not yet been analyzed globally. In this study, we performed transomic analysis, including transcriptomics and metabolomics, of glucose-responsive molecules in the skeletal muscle of WT and leptin-deficient obese mice (*ob*/*ob* mice) mice during oral glucose administration. Leptin is an anorexigenic hormone, and the *ob*/*ob* mice exhibits profound obesity by overeating. By analyzing time-series data, we identified pathways that are activated or inhibited by oral glucose administration, and determined how they are dysregulated in obesity. Our study provides a better understanding of the mechanism of glucose metabolism in skeletal muscle and T2DM.

Results

Overview of the study.

Metabolic reactions, which are defined as chemical reactions of metabolism, are regulated by an integrated network of metabolites as allosteric regulators, substrates, and products; metabolic enzymes; transcription factors; and signaling molecules. To elucidate the regulatory network controlling glucose-responsive metabolic reactions in skeletal muscle, we constructed a regulatory transomic network by integrating metabolic reactions with metabolites, gene expression of metabolic enzymes, and transcription factors, using skeletal muscle excised from C57BL/6J WT mice or *ob*/*ob* mice at different time points after glucose administration (Fig. S1). The transomic network of the skeletal muscle was constructed according to our previous study of the liver[12].

Glucose was administered orally to 16 h-fasted WT and *ob*/*ob* mice, and the gastrocnemius muscle and blood were collected at 0, 20, 60, 120, and 240 min after glucose administration (Fig. 1A). The *ob*/*ob* mice showed elevated levels of blood glucose and insulin compared to WT mice throughout the study (Fig. S2A). The blood and skeletal muscle data in the fasting state were obtained from our previous studies[12,13]. The skeletal muscle data after oral glucose administration were newly obtained in this study (Fig. S2B).

Using the skeletal muscle data during oral glucose administration, we defined the features of glucose-responsive molecules according to our previous study[12]. Molecules that showed statistically significant changes (absolute $\log_2$ fold change ≥ 0.585 [$2^{0.585} = 1.5$] and a false discovery rate [FDR]-adjusted p value [q value] ≤ 0.1) at any time point compared to the fasting state after glucose administration were defined as glucose-responsive (Fig. 1B). We also calculated time constants ($T_{1/2}$) to study the temporal patterns of glucose-responsive molecules (Fig. 1C). $T_{1/2}$ was defined as the amount of time needed for the response to reach half of the minimum (decreasing molecules) or maximum (increasing molecules) amplitude. According to the blood insulin concentration, which peaked at about 20 min and decreased to basal level at about 60 min (Fig. S2A), rapid responses were defined as those with $T_{1/2}$ values less than 20 min, and slow responses were defined as those with values longer than 60 min.

Glucose-responsive molecules were integrated across the omic layers, and the regulatory transomic network was constructed in WT and *ob*/*ob* mice (Fig. 1A). The transomic networks contained layers of insulin signaling molecules (Insulin signal), transcription factors (TF), gene expression and phosphorylation of metabolic enzymes (Enzyme), metabolic reactions (Reaction), and metabolites (Metabolite), and the layers were connected when regulations could be speculated. By comparing the regulatory transomic networks between WT and *ob*/*ob* mice, we comprehensively evaluated how obesity affects the responses to glucose in skeletal muscle.

Metabolomics.

We first performed metabolomics analysis using capillary electrophoresis–mass spectrometry (CE–MS), liquid chromatography (LC) –MS, and enzyme assays. A total of 104 water-soluble and ionic metabolites including glucose, amino acids, and nucleic acids were measured by CE–MS. Statistical tests were

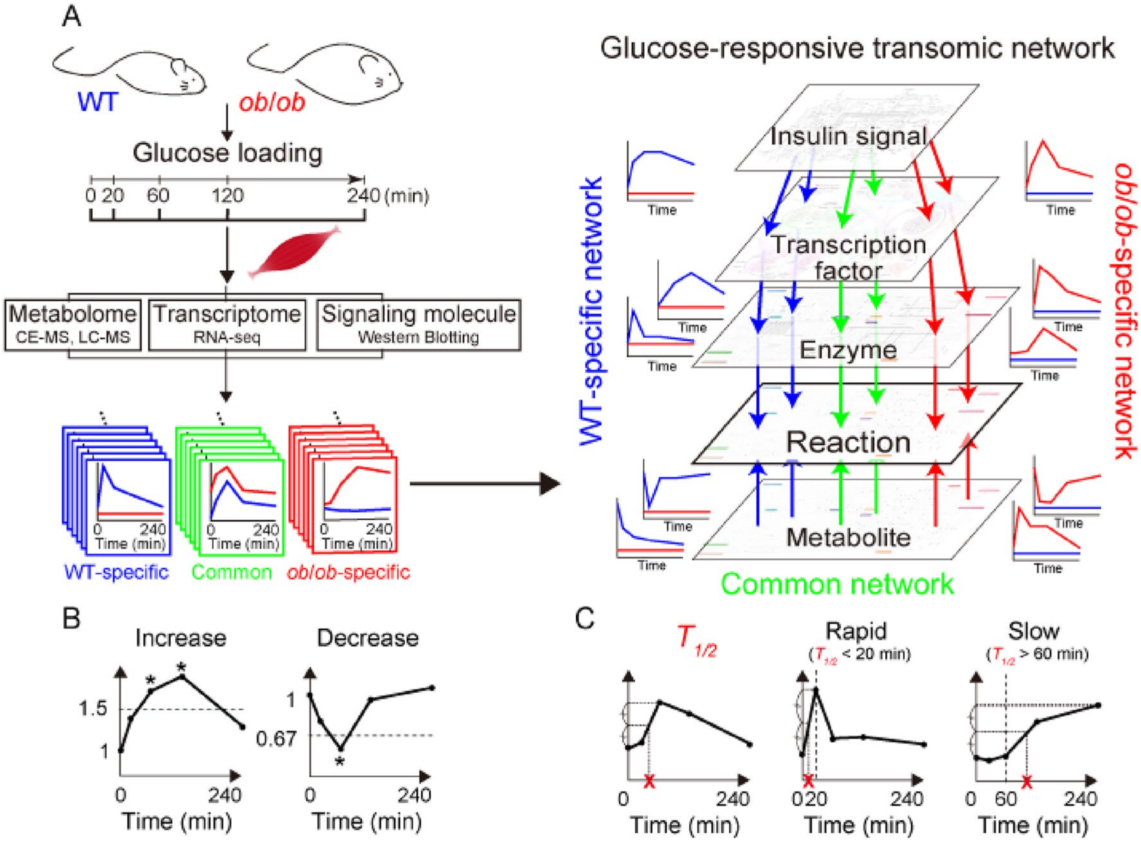
A
WT
ob/ob
Glucose loading
0 20 60 120 240 (min)
Metabolome
CE-MS, LC-MS
Transcriptome
RNA-seq
Signaling molecule
Western Blotting
0 240
Time (min)
WT-specific
Common
ob/ob-specific
Glucose-responsive transomic network
Insulin signal
Transcription factor
Enzyme
Reaction
Metabolite
Time
WT-specific network
ob/ob-specific network
Common network
B
Increase
Decrease
1.5
1
0.67
0 240
Time (min)
C
T1/2
Rapid
(T1/2 < 20 min)
Slow
(T1/2 > 60 min)
0 20 60 240
Time (min)

Figure 1. Pipeline of the construction of the glucose-responsive transomic network. (**A**) We measured the time courses of multiomic data from the skeletal muscles of WT and *ob*/*ob* mice following oral glucose administration and identified the molecules that were changed by oral glucose administration, which we defined as glucose-responsive molecules in each layer. We addedinterlayer regulatory connections between glucose-responsive molecules in different layers using bioinformatics methods and information in public databases. The result was a glucose-responsive transomic network in the skeletal muscle of WT and *ob*/*ob* mice. We identified transomic subnetworks specific to WT mice (blue), *ob*/*ob* mice (red), and common to both mice (green). (**B**) Definition of glucose-responsive molecules using fold change and FDR-adjusted p value (q value). *q value < 0.1 and absolute $\log_2$ fold change > 0.585. (**C**) Definition of $T_{1/2}$, an index of the temporal rate of response, and rapid and slow glucose-responsive molecules using $T_{1/2}$. This figure was modified from Figure 1 of Kokaji et al. (2020).

performed to identify the glucose-responsive metabolites in WT and *ob*/*ob* mice (Fig. 2A,B; Data File S1). To define an increase or decrease in time courses with changes in both directions at different time points, the direction of change compared to time 0 at the earliest time point that showed a significant change was used. Metabolites that showed statistically significant increases or decreases in WT or *ob*/*ob* mice are shown in Fig. 2A. The responses were categorized into three groups (rapid, intermediate, or slow) according to their $T_{1/2}$ values (Fig. 2C).

Four metabolites (4% of the total quantified metabolites) were significantly increased only in *ob*/*ob* mice, and none were increased in WT mice (Fig. 2B). Metabolites that were increased only in *ob*/*ob* mice included fructose 6-phosphate (F6P), tartrate, lactate, and isoamylamine (Fig. 2D). Twenty-one metabolites (20%) were significantly decreased only in WT mice, and four metabolites (4%) were significantly decreased only in *ob*/*ob* mice (Fig. 2B). It is noteworthy that no common metabolites were increased or decreased in WT and *ob*/*ob* mice. Metabolites decreased in WT mice included those that play a role in the tricarboxylic acid (TCA) cycle, such as citrate, cis-aconitate, succinate, and malate (Fig. 2D). The ketone body 3-hydroxybutylate (3-OH-butylate) was also decreased in WT mice. Metabolites that were decreased in *ob*/*ob* mice included valine, aspartic acid, choline, and 3-methylhistidine. Most of the decreased metabolites showed rapid responses in both WT and *ob*/*ob* mice (Fig. 2C). Hierarchical clustering analysis of the metabolites is shown in Figure S3. LC–MS did not detect significant responses of 14 lipids after oral glucose administration (Data File S2).

Our metabolomic analysis revealed that the number of glucose-responsive metabolites specific to WT mice (21: 0 increased + 21 decreased) was larger than that specific to *ob*/*ob* mice (8: 4 increased + 4 decreased), and no responses were common to both mice. These results indicate that there is a substantial difference in the mechanism of glucose metabolism in skeletal muscle between WT and *ob*/*ob* mice.

Next, we compared the metabolomic changes in the skeletal muscle and blood. The amount of metabolites was regulated not only within each organ but in the blood circulatory system[14]. For each metabolite that was measurable in both skeletal muscle and blood (61 metabolites), we calculated the correlation between the time course of

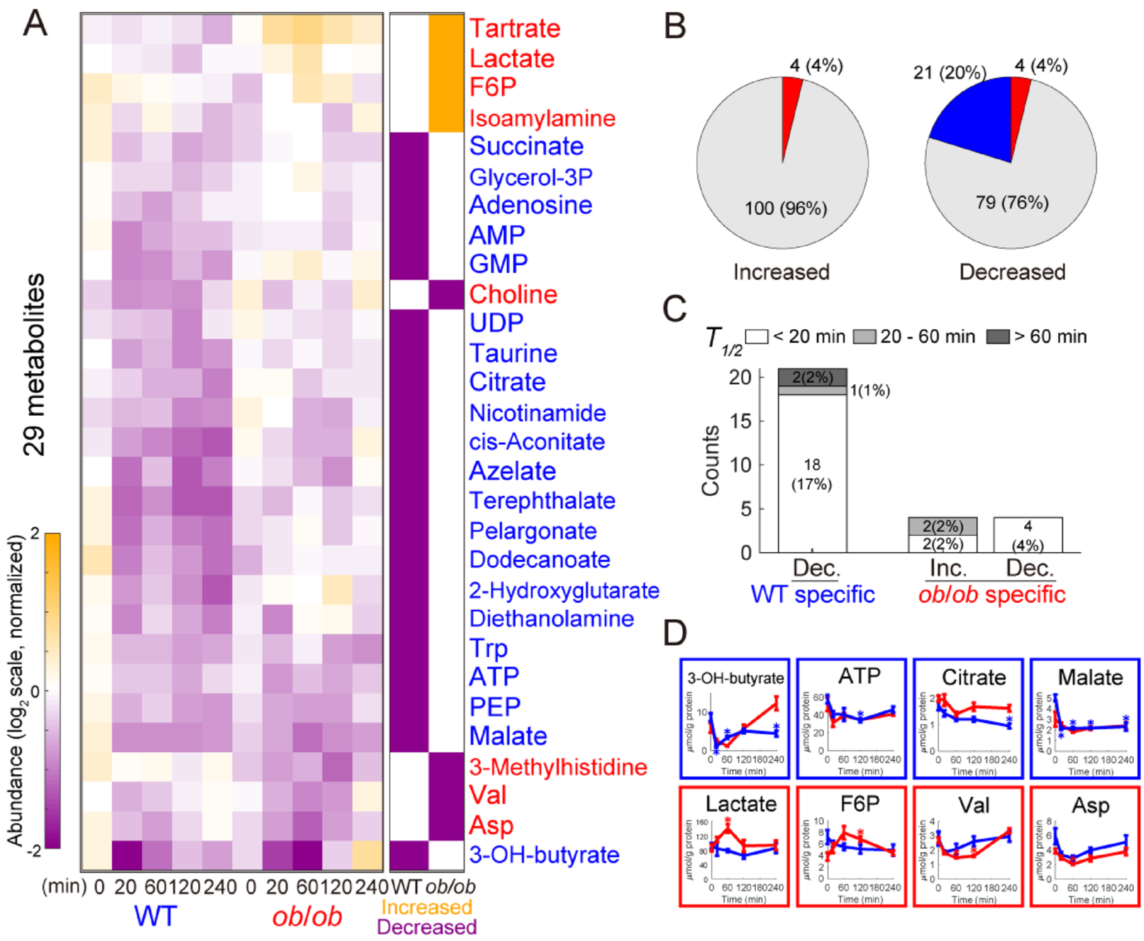

Figure 2. Identification of glucose-responsive metabolites. (**A**) Left: Heat map of the time courses of 29 glucose-responsive metabolites from the skeletal muscles of WT and *ob*/*ob* mice following oral glucose administration (n = 5 mice per genotype at all time points). To investigate the changes from fasting state, two time courses for each metabolite were divided by the geometric mean of the values of fasted WT mice and *ob*/*ob* mice (0 min) and then $\log_2$-transformed. Metabolites were ordered by hierarchical clustering using Euclidean distance and Ward's method. Right: The bars in the heat map are colored according to the extent of glucose responsiveness, meaning the change from fasting state (0 min) in WT and *ob*/*ob* mice. Metabolites that showed an absolute $\log_2$ fold change ≥ 0.585 ($2^{0.585} = 1.5$) and an FDR-adjusted *p* value (q value) ≤ 0.1 at any time point (20, 60, 120, 240 min) were defined as glucose-responsive: increased (orange), decreased (purple), or were unchanged (white). To define an increase or decrease in time courses with changes in both directions at different times, we used the direction of change compared to time 0 at the earliest time point that showed a significant change. Metabolites written in blue text indicate glucose-responsive metabolites specific to WT mice; red text, specific to *ob*/*ob* mice. (**B**) Increased and decreased metabolites in the skeletal muscles of WT mice and *ob*/*ob* mice. Blue, WT specific; red, *ob*/*ob* specific; gray, not glucose-responsive metabolites either in WT mice or in *ob*/*ob* mice. The number of each type of glucose-responsive metabolites and their percentages of the total quantified metabolites are shown. (**C**) Rapid, intermediate, and slow responses in increased metabolites specific to WT mice, decreased metabolites specific to WT mice, increased metabolites specific to *ob*/*ob* mice, and decreased metabolites specific to *ob*/*ob* mice. (**D**) Graphs showing the metabolites with responses that were specific to WT mice (blue boxes) and specific to *ob*/*ob* mice (red boxes). Blue lines are the responses of the WT mice and red lines are the responses of the *ob*/*ob* mice. Data are shown as the mean and standard error of the mean (SEM) of five mice per genotype. *q value < 0.1 and absolute $\log_2$ fold change > 0.585. Metabolites are abbreviated as follows: F6P, fructose 6-phosphate; PEP, phosphoenolpyruvate; Glycerol-3P, glycerol 3-phosphate; 3-OH-butyrate, 3-hydroxybutanoate.

the metabolites in the skeletal muscle and that in the blood (Fig. S4A). The blood data were obtained from our previous study[12]. The decreases in 3-OH-butyrate, isoleucine, and leucine were highly correlated between the blood and muscle in WT mice; and the decreases in 3-OH-butyrate and increases in lactate were highly correlated between the blood and muscle in *ob*/*ob* mice (Fig. S4A, B). Our previous study showed that 3-OH-butyrate, isoleucine, and leucine also exhibited a high correlation between the blood and liver in the same mouse[12]. These results suggest that metabolites regulated in the bloodstream are regulated similarly in skeletal muscle and liver.

Transcriptomics. To elucidate the transcriptional changes and controls in the skeletal muscle of WT and *ob*/*ob* mice after glucose administration, we performed transcriptomic analysis using RNA sequencing. Of the 14,978 genes analyzed, 4,264 that were significantly changed after oral glucose administration were identified as glucose-responsive genes (Fig. 3A,B; Data File S3). A heatmap of the glucose-responsive genes is shown in Fig. 3A. The responses were categorized into three groups (rapid, intermediate, or slow) according to their $T_{1/2}$ s as in the analysis of the metabolites (Fig. 3C,D). Pathway enrichment analysis was also performed for each type of response (Table 1 and Data File S4). We assigned glucose-responsive genes encoding metabolic enzymes to the Enzyme layer of the transomic network, and glucose-responsive genes encoding transcription factors to the TF layer of the transomic network (Figs. 1 and 5).

The number of upregulated and downregulated genes in WT and *ob*/*ob* mice is shown in Fig. 3B. The number of glucose-responsive genes specific to *ob*/*ob* mice (1414 upregulated, 995 downregulated) was larger than that specific to WT mice (624 upregulated, 472 downregulated). A total of 637 common genes were upregulated and 264 were downregulated in WT and *ob*/*ob* mice. The calculation of time constants revealed that the number of rapidly responding glucose-responsive genes was larger in *ob*/*ob* mice than in WT mice (Fig. 3C). Genes upregulated in both WT and *ob*/*ob* mice included those involved in central carbon metabolism, such as hexokinase 2 (*Hk2*), fatty acid synthase (*Fasn*), and stearoyl-coenzyme A (CoA) desaturase 1(*Scd1*), and the responses in *ob*/*ob* mice were larger than those in WT mice (Fig. 3E). Some genes involved in the insulin signaling pathway also showed upregulation common to both WT and *ob*/*ob* mice, such as insulin receptor substrate 1 (*Irs1*) and nitric oxide synthase 3 (*Nos3*) (Fig. 3E). Genes downregulated in both WT and *ob*/*ob* mice included those involved in oxidative phosphorylation such as NADH dehydrogenase (ubiquinone) iron-sulfur protein 4 (*Ndufs4*) (Fig. 3E). Genes specifically downregulated in WT mice contained pyruvate dehydrogenase kinase 4 (*Pdk4*) (Fig. 3E). Genes specifically upregulated in *ob*/*ob* mice were relatively enriched in pathways related to cell adhesion (Table 1). The gene 3-hydroxybutyrate dehydrogenase 1 (*Bdh1*), which is involved in ketone body metabolism, was also specifically upregulated in *ob*/*ob* mice. Genes specifically downregulated in *ob*/*ob* mice included those involved in the TCA cycle such as succinyl-CoA synthetase beta subunit (*Suclg2*), and those involved in branched-chain amino acid (BCAA) degradation such as 2-oxoisovalerate dehydrogenase beta subunit (*Bckdhb*) (Fig. 3E). Genes specifically downregulated in *ob*/*ob* mice were relatively enriched in the proteasome pathway and ribosomal proteins (Table 1).

Next, we performed hierarchical clustering analysis of transcriptome data and bioinformatics analysis of the binding motifs of gene clusters using the transcription factor database TRANSFAC (Figs. 3E and S5A, B; Data Files S5 and S6) to estimate the regulatory connections between transcription factors and genes[15,16]. We predicted the regulatory connections between a transcription factor and a gene if the binding motifs of the transcription factor were enriched in the promoter regions of the genes in a cluster. For example, we inferred that early growth response protein 1 (Egr1) is a transcription factor that regulates some of the genes upregulated in WT and *ob*/*ob* mice (Fig. 3E). A comparison of the estimated regulatory connections with those predicted from chromatin immunoprecipitation (ChIP) experimental data from the ChIP-Atlas database (http://chip-atlas.org/)[17] showed that the results from the two methods mostly overlapped (Fig. S5C; Data File S7). The estimated regulatory connections between the transcription factors and the genes encoding metabolic enzymes acted as connections between the TF layer and the Enzyme layer in the transomic network.

Phosphorylation of insulin signaling molecules. Phosphorylation is an important factor for regulating metabolic reactions. Direct phosphorylation of an enzyme can regulate its activity, and phosphorylation of a transcription factor can regulate the expression level of downstream enzymes. Therefore, we measured the phosphorylation of 10 enzymes, transcription factors, and signaling molecules in the insulin pathway by performing western blot analysis of protein samples prepared from the skeletal muscle of WT and *ob*/*ob* mice during oral glucose administration (Fig. S6; Data File S8). The band intensities were quantified, and the results were used to determine if the phosphorylation was glucose-responsive.

We were able to detect many glucose-responsive phosphorylated proteins from the analysis (Fig. 4). The level of phosphorylated ribosomal protein S6 was increased in both WT and *ob*/*ob* mice. Phosphorylated Akt was specifically increased in WT mice, and phosphorylated glycogen phosphorylase was specifically decreased in WT mice. Glycogen synthase kinase 3 β (Gsk3β) and cAMP response element-binding protein (Creb) were specifically increased in *ob*/*ob* mice. Some molecules showed the opposite responses in WT and *ob*/*ob* mice. For example, phosphorylated forkhead box protein 1 (Foxo1) was transiently increased in WT mice but decreased in *ob*/*ob* mice; phosphorylated glycogen synthase (Gs) was decreased in WT mice and increased in *ob*/*ob* mice. Phosphorylated extracellular signal-related kinase (Erk) and AMP-activated protein kinase α (Ampkα) was not affected by glucose administration in both WT and *ob*/*ob* mice. In the subsequent transomic analysis, metabolic enzymes with glucose-responsive phosphorylation were assigned to the Enzyme layer, and transcription factors with glucose-responsive phosphorylation were assigned to the TF layer.

Regulatory glucose-responsive transomic network. A regulatory transomic network of glucose-responsive molecules in the skeletal muscle was constructed with five layers: Insulin signal, TF, Enzyme, Reaction, and Metabolite (Fig. 5; Data File S9). We constructed the transomic network in the skeletal muscle using a method we previously developed for the transomic network in the liver[12]. Briefly, glucose-responsive molecules were assigned to the corresponding layers as nodes, and the edges between the nodes were drawn to show the interlayer regulatory connections of glucose-responsive molecules retrieved from pathway databases such as Kyoto Encyclopedia of Genes and Genomes (KEGG) and Braunschweig Enzyme Database (BRENDA)[18–20] (Fig. 5A).

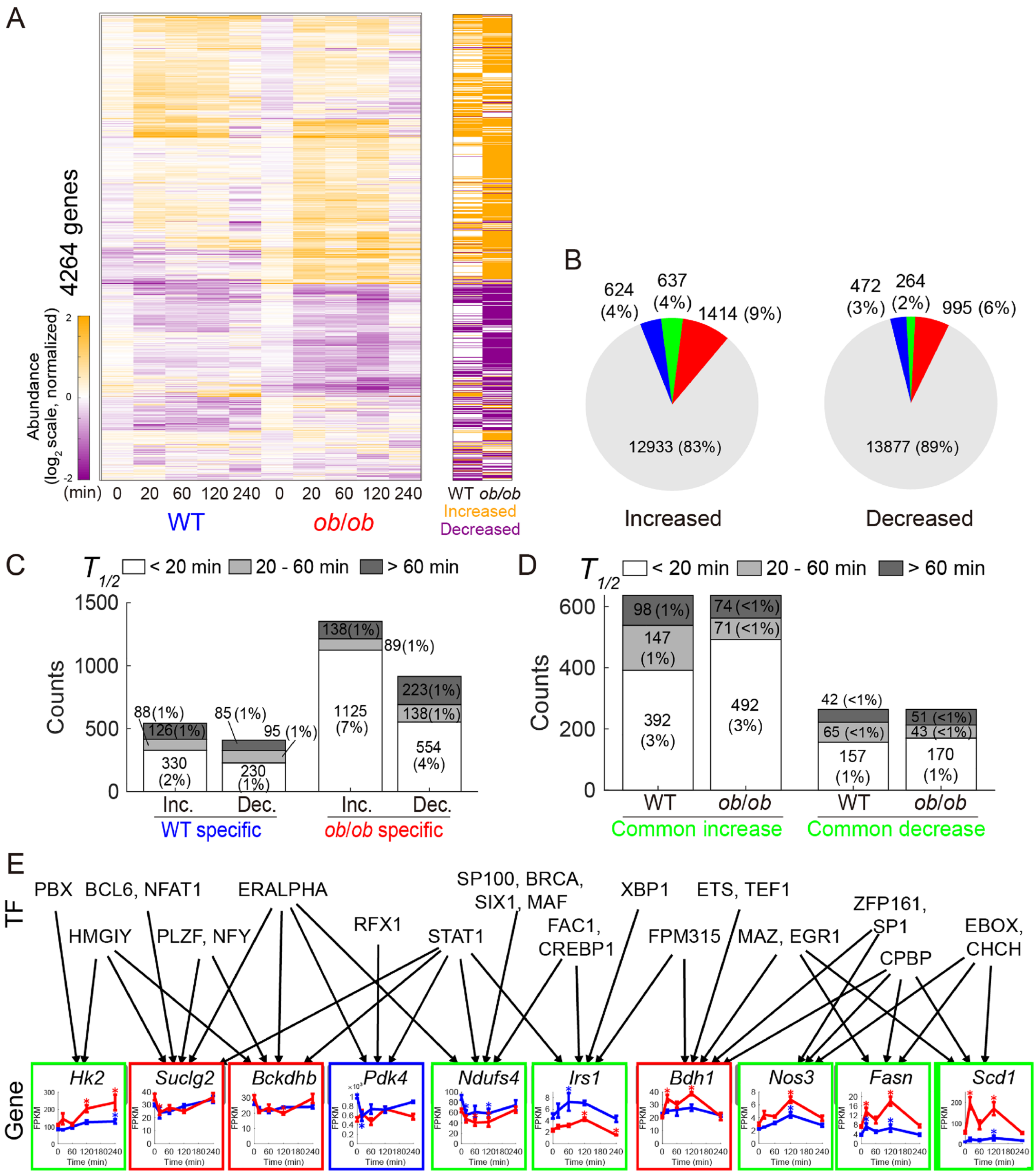
A
4264 genes
Abundance (log$_2$ scale, normalized)
2
0
-2
(min) 0 20 60 120 240 0 20 60 120 240
WT
ob/ob
WT ob/ob
Increased
Decreased
B
624 (4%)
637 (4%)
1414 (9%)
12933 (83%)
Increased
472 (3%)
264 (2%)
995 (6%)
13877 (89%)
Decreased
C
$T_{1/2}$ ▢ < 20 min ▨ 20 - 60 min ■ > 60 min
Counts
1500
1000
500
0
88(1%)
126(1%)
330 (2%)
85(1%)
95 (1%)
230 (1%)
138(1%)
89(1%)
1125 (7%)
223(1%)
138(1%)
554 (4%)
Inc.
Dec.
Inc.
Dec.
WT specific
ob/ob specific
D
$T_{1/2}$ ▢ < 20 min ▨ 20 - 60 min ■ > 60 min
Counts
600
400
200
0
98 (1%)
147 (1%)
392 (3%)
74 (<1%)
71 (<1%)
492 (3%)
42 (<1%)
65 (<1%)
157 (1%)
51 (<1%)
43 (<1%)
170 (1%)
WT
ob/ob
WT
ob/ob
Common increase
Common decrease
E
TF
PBX
BCL6, NFAT1
ERALPHA
SP100, BRCA, SIX1, MAF
XBP1
ETS, TEF1
ZFP161, SP1
EBOX, CHCH
HMGIY
PLZF, NFY
RFX1
STAT1
FAC1, CREBP1
FPM315
MAZ, EGR1
CPBP
Gene
Hk2
Suclg2
Bckdhb
Pdk4
Ndufs4
Irs1
Bdh1
Nos3
Fasn
Scd1
FPKM
Time (min)
0 60 120 180 240

◂**Figure 3.** Identification of glucose-responsive genes. (**A**) Left: Heat map of the time courses of transcript abundance for 4,264 glucose-responsive genes in the skeletal muscles of WT and *ob*/*ob* mice following oral glucose administration (n = 11 or 12 mice per genotype at 0 min, n = 5 mice per genotype at 20 min, n = 5 mice per genotype at 60 min, n = 5 mice per genotype at 120 min, and n = 5 mice per genotype at 240 min). To investigate the changes from fasting state, two time courses for each gene were divided by the geometric mean of the values of WT mice and *ob*/*ob* mice in the fasting state (0 min), and then $\log_2$-transformed. Genes were ordered by hierarchical clustering using Euclidean distance and Ward's method (Data File S3). Right: The bars in the heat map are colored according to glucose responsiveness, meaning the change from fasting state (0 min) in WT and *ob*/*ob* mice. Genes that showed an absolute $\log_2$ fold change ≥ 0.585 ($2^{0.585} = 1.5$) and a q value ≤ 0.1 at any time point (20, 60, 120, 240 min) were defined as glucose-responsive: upregulated (orange), downregulated (purple), or were unchanged (white). (**B**) Increased and decreased genes in the skeletal muscle of WT mice and *ob*/*ob* mice. Blue, WT specific; red, *ob*/*ob* specific; green, glucose-responsive genes common to both; gray, not glucose-responsive metabolites either in WT mice or in *ob*/*ob* mice. The number of each type of glucose-responsive genes and their percentages out of the total quantified genes are shown. (**C**) Rapid, intermediate, and slow responses in increased genes specific to WT mice, decreased genes specific to WT mice, increased genes specific to *ob*/*ob* mice, and decreased genes specific to *ob*/*ob* mice. (**D**) Rapid, intermediate, and slow responses in increased and decreased genes common to both WT and *ob*/*ob* mice. (**E**) Graphs showing the gene expression time courses for the indicated genes. Genes include those that exhibited changes in common to both WT and *ob*/*ob* (green boxes), changes specific to WT mice (blue box), and changes specific to *ob*/*ob* mice (red boxes). Within the graphs, blue lines are the responses of the WT mice and red lines are the responses of the *ob*/*ob* mice. The inferred regulatory connections are shown as arrows from transcription factors to genes. The regulatory connections were inferred using hierarchical clustering analysis of gene expression time courses together with a transcription factor database TRANSFAC[15,16]. See Figure S5 for statistical confidence in the inferred transcription factors; see Data File S5 for the unabbreviated names of the transcription factors. Data are shown as the mean and SEM (n = 11 or 12 mice per genotype at 0 min, n = 5 mice per genotype at 20 min, n = 5 mice per genotype at 60 min, n = 5 mice per genotype at 120 min, and n = 5 mice per genotype at 240 min). *q value < 0.1 and absolute $\log_2$ fold change > 0.585.

By constructing regulatory transomic networks in WT and *ob*/*ob* mice, we were able to identify WT specific, *ob*/*ob* specific, and common responses of molecules and interlayer regulatory connections to glucose administration (Fig. 5B; green, common; blue, WT specific; red, *ob*/*ob* specific). In the Metabolite layer, the number of WT mice specific glucose-responsive molecules was larger than *ob*/*ob* mice specific glucose-responsive molecules, and no molecules responded commonly in WT and *ob*/*ob* mice. Therefore, most of the interlayer regulatory connections between the Metabolite layer and the Reaction layer were specific to WT mice, suggesting that metabolic regulation by a metabolite itself after glucose administration is impaired in obesity. By contrast, approximately 55% of glucose-responsive genes in the Enzyme layer and the interlayer regulatory connections between the Enzyme layer and the Reaction layer were classified as *ob*/*ob* specific, suggesting that transcriptional regulation compensated for the regulation by metabolites that was lost in obese mice. The number of common glucose-responsive genes in the Enzyme layer and its regulatory connections was approximately 40% of the *ob*/*ob* specific ones.

The numbers of glucose-responsive metabolic reactions regulated by metabolites (Metabolite layer), genes (Enzyme layer), or both were calculated (Fig. 5C). The results suggested that the metabolic reactions in WT mice were mainly regulated by metabolites, and those in *ob*/*ob* mice were mainly regulated through gene expression. We also classified the regulators of metabolic reactions according to their time constants ($T_{1/2}$), and revealed that a large number of metabolic reactions was affected by the rapidly responding (<20 min) metabolites and genes in both the WT and *ob*/*ob* networks (Fig. 5D). Glucose-responsive metabolites specific to WT mice included cofactors such as ATP, AMP, and UDP, which could have a large effect on the Reaction layer (Fig. 5E).

Comparison of the regulatory transomic networks of WT and *ob*/*ob* mice.

To analyze how each metabolic pathway was regulated in the regulatory transomic networks of WT and *ob*/*ob* mice, we constructed a simplified transomic network using a method that we previously developed[12] (Fig. 6; Data File S10). Briefly, we converted the Reaction layer into the Pathway layer by placing metabolic reactions in a specific metabolic pathway into a single metabolic pathway node, according to the KEGG metabolic pathway.

In WT mice, various metabolic pathways were regulated by metabolites (Fig. 6A). In particular, carbohydrate metabolic pathways were regulated by WT specific glucose-responsive metabolites such as ATP, citrate, and phosphoenolpyruvate (PEP). Although the effects of glucose-responsive genes encoding metabolic enzymes were smaller than the metabolites, some lipid metabolic pathways such as glycerolipid and glycerophospholipid metabolisms were more strongly regulated by glucose-responsive genes than others (Fig. S7A). In *ob*/*ob* mice, the regulation of glucose-responsive metabolites was decreased and that of glucose-responsive genes encoding metabolic enzymes was increased (Fig. 6B). The decreased regulation by metabolites was particularly large in carbohydrate metabolic pathways (Fig. S7A). Regulation by glucose-responsive genes was increased in most carbohydrate and lipid metabolic pathways, with the exception of glycerolipid metabolism. Amino acid metabolic pathways showed relatively small changes in the percentage of metabolic reactions regulated by glucose-responsive metabolites and genes.

Glycolysis, TCA cycle, BCAA degradation, and ketone body metabolism.

Finally, we focused on metabolic pathways and their regulatory networks related to glucose (Fig. 7).

	Upregulated gene in WT		**Downregulated gene in WT**		**Unchanged gene in WT**			
	Activity	***p* value**	**Activity**	***p* value**	**Activity**	***p* value**	**Activity**	***p* value**
Upregulated gene in *ob*/*ob*	Adherens junction	8.1×10^{-3}			Gap junction	1.1×10^{-3}	Focal adhesion	8.8×10^{-3}
	Butirosin and neomycin biosynthesis	9.4×10^{-3}			Adherens junction	2.8×10^{-3}	Regulation of actin cytoskeleton	1.2×10^{-2}
					Glycosaminoglycan biosynthesis—heparan sulfate/heparin	5.6×10^{-3}	Glycosaminoglycan biosynthesis—chondroitin sulfate/dermatan sulfate	2.0×10^{-2}
					Signaling pathways regulating pluripotency of stem cells	6.3×10^{-3}		
Downregulated gene in *ob*/*ob*			Histidine metabolism	3.6×10^{-2}	Proteasome	2.7×10^{-3}	Mismatch repair	3.7×10^{-2}
					Ribosome	1.0×10^{-2}	Retinol metabolism	4.3×10^{-2}
					Arachidonic acid metabolism	2.5×10^{-2}	Drug metabolism—other enzymes	4.9×10^{-2}
					Non-homologous end-joining	3.0×10^{-2}		
Unchanged gene in *ob*/*ob*	Histidine metabolism	3.0×10^{-3}	Taurine and hypotaurine metabolism	1.3×10^{-2}				
	Phenylalanine metabolism	1.2×10^{-2}	Drug metabolism—other enzymes	2.4×10^{-2}				
	beta-Alanine metabolism	1.4×10^{-2}						

Table 1. Pathway enrichment analysis of the glucose-responsive genes. Pathways with p value < 0.05 are shown.

Glycolysis. In WT mice, although blood glucose levels increased after glucose administration, most metabolites in glycolysis were not defined as "glucose-responsive." The glycolysis network contained many allosteric inhibitors that decreased specifically in WT mice, such as ATP and citrate (Fig. 7A). We also found upregulation in some glycolytic genes such as *Hk2*, and downregulation in *Pdk4*, which inhibits pyruvate dehydrogenase by phosphorylation[21].

In *ob*/*ob* mice, F6P and lactate were defined as specifically increased metabolites, and some gene expression such as *Hk2* showed a larger increase than in WT mice. Most of the responses of allosteric regulators of glycolysis were lost in *ob*/*ob* mice. . Glucose 6-phosphate (G6P) was not defined as a glucose-responsive molecule (q value at 60 min = 0.14), but its time series was highly correlated with F6P (Pearson's r = 0.99).

TCA cycle. In WT mice, four metabolites in the TCA cycle, namely citrate, cis-aconitate, succinate, and malate, decreased after oral glucose administration (Fig. 7B). Although fumarate was not defined as a glucose-responsive molecule (q value at 60 min = 0.13), its time series was highly correlated with malate (Pearson's r = 0.96)[21–24]. In *ob*/*ob* mice, the abundance of some metabolites was smaller than that in WT mice before glucose administration, and the metabolites did not show a large response to glucose. Some studies have reported a decrease in intermediates of the TCA cycle in the skeletal muscle of obese mice[25,26].

BCAA degradation. BCAA degradation pathway and its regulatory network included some glucose-responsive molecules in *ob*/*ob* mice (Fig. 7C). Valine showed a rapid decrease after oral glucose administration. Leucine and isoleucine were not defined as glucose-responsive molecules (q value at 20 min = 0.15, 0.16), but their time series were highly correlated with valine (Pearson's r = 0.98 for leucine, 0.98 for isoleucine). Some genes involved in BCAA degradation, such as *Bckdhb*, showed a rapid downregulation. Bckdh kinase (Bckdk) inhibits Bckdh by phosphorylation[27], which was not defined as a glucose-responsive molecule (q value at 60 min = 0.11), but its time series was negatively correlated with *Bckdhb* expression (Pearson's r = -0.96). We found a similar decrease in *Suclg2* in the TCA cycle, which metabolizes succinyl CoA, one of the BCAA degradation products (Fig. 7B). In WT mice, BCAAs were not defined as glucose-responsive molecules (q value at 20 min = 0.15 to 0.23), but their time series showed a positive correlation with those in *ob*/*ob* mice (Pearson's r = 0.77 to 0.90). Acyl-CoA dehydrogenase short/branched chain (*Acadsb*), methylcrotonoyl-CoA carboxylase 2 (*Mccc2*), and *Suclg2* showed significant decrease in WT mice, but only *Acadsb* was defined as glucose-responsive because of its fold changes (fold change at 20 min = 0.64, 0.76, 0.80).

Ketone body metabolism. In WT mice, 3-OH butyrate, a ketone body, showed a rapid and strong decrease (0.13-fold at 20 min) (Fig. 7D). The network included the decreases in metabolites in the TCA cycle as allosteric inhibitors of the metabolic enzyme that degrades acetoacetate. In *ob*/*ob* mice, 3-OH butyrate did not show a significant decrease (q value at 60 min = 0.12), but *Bdh1* was rapidly upregulated.

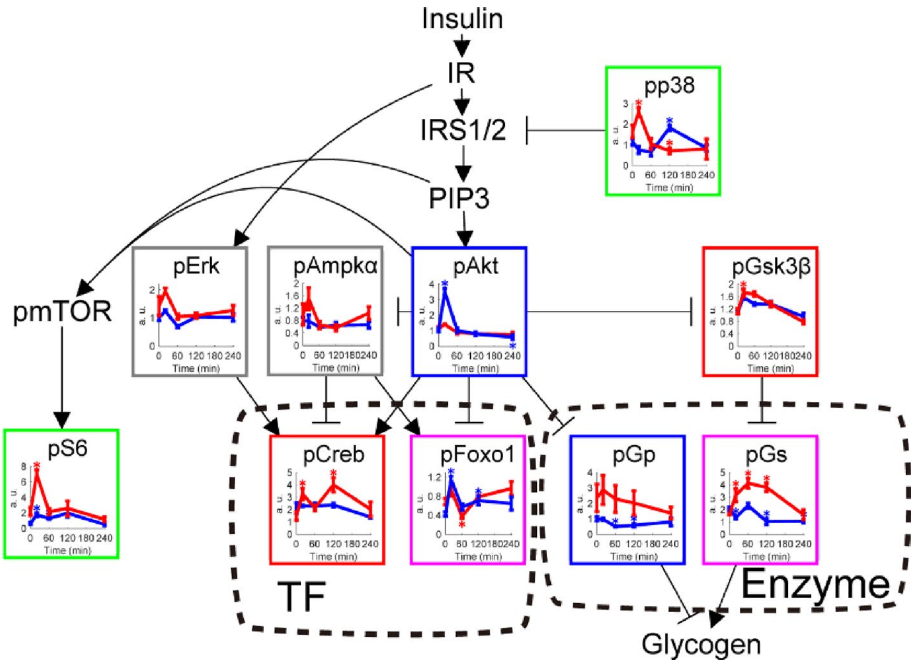

Figure 4. Identification of glucose-responsive phosphorylation of insulin signaling molecules. Time courses of the amount and phosphorylation of the indicated insulin signaling molecules in the skeletal muscle of WT mice (blue lines) and *ob*/*ob* mice (red lines) following oral glucose administration. Phosphorylated proteins are indicated by the prefix "p." The time course graphs are presented in the context of the insulin signaling pathway from the KEGG database[18,19]. Edges reflect direct or indirect regulatory events. Not all molecules in this pathway are shown. The nodes without time course graph (insulin receptor [IR], insulin receptor substrate 1/2 [IRS1/2], phosphatidyl-inositol 3,4,5-trisphosphate [PIP3], and mammalian target of rapamycin [mTOR]) were not quantified here. The colors of the boxes around each graph indicate the change in amount or phosphorylation specific to WT (blue), specific to *ob*/*ob* (red), common to both (green), opposite between WT and *ob*/*ob* mice (pink). Proteins that did not exhibit a change in phosphorylation are outlined in gray. Proteins that showed an absolute $\log_2$ fold change ≥ 0.585 ($2^{0.585} = 1.5$) and a q value ≤ 0.1 at any time point (20, 60, 120, 240 min) were defined as glucose-responsive. Glucose-responsive molecules in the TF and Enzyme layers are enclosed in dashed boxes. See Data File S8 for the unabbreviated names of the insulin signaling molecules. Data are shown as the mean and SEM of five mice per genotype (see Fig. S6 for Western blot). *q value < 0.1 and absolute $\log_2$ fold change > 0.585.

Discussion

In this study, we performed transomic analysis of the skeletal muscles obtained from WT and *ob*/*ob* mice after the oral glucose tolerance test to construct a large-scale glucose-responsive regulatory network of metabolism. In WT mice, the number of glucose-responsive metabolites was about 2.5-fold larger than that in *ob*/*ob* mice, and many metabolic reactions were affected by these glucose-responsive metabolites. In particular, the responses of cofactors such as ATP, and TCA cycle intermediates such as citrate and succinate, might affect carbohydrate and amino acid metabolism. By contrast, the number of glucose-responsive genes encoding metabolic enzymes in *ob*/*ob* mice was about 1.8-fold larger than that in WT mice, and the genes were mainly related to carbohydrate and lipid metabolism.

We also found some characteristic glucose-responsive regulatory pathways in central carbon, branched amino acids, and ketone body metabolism. The WT mice showed few significant changes in the metabolites of glycolysis despite the administration of glucose. This can be attributed to two hypotheses. The first hypothesis is that the influx into the muscle glycolytic system does not increase as much as the blood glucose levels. A recent study showed that the influx of orally administered labelled glucose into the glycolysis of gastrocnemius muscle (white muscle), which was used in this study, is much smaller than that of soleus muscle (red muscle)[28]. The second hypothesis is that the efflux of glycolysis increased by activation as much as the influx. Thus, the network of glycolysis in WT mice included some activating regulatory pathways, such as the decrease of allosteric inhibitor including ATP and TCA cycle intermediates, the upregulation of glycolytic genes, and the downregulation of *Pdk4* (Fig. 7A), which could contribute to blood glucose homeostasis after glucose administration. Because blood lactate increased (Fig. S4B), much of the increased glucose flowed into glycolysis after administration might be released into the blood as lactate[29,30]. This is consistent with the decrease in ATP and TCA cycle intermediates, which suggests a decrease in TCA cycle flux (Fig. 7B). By contrast, *ob*/*ob* mice showed the considerable increase in F6P and G6P, suggesting that the conversion from glucose to G6P was activated in response to blood glucose levels, but to a lesser extent in the glycolytic system. Consistently, in *ob*/*ob* mice, most of allosteric activation of glycolysis was lost, and *Hk2* showed larger increase than WT mice, which could be compensational regulation

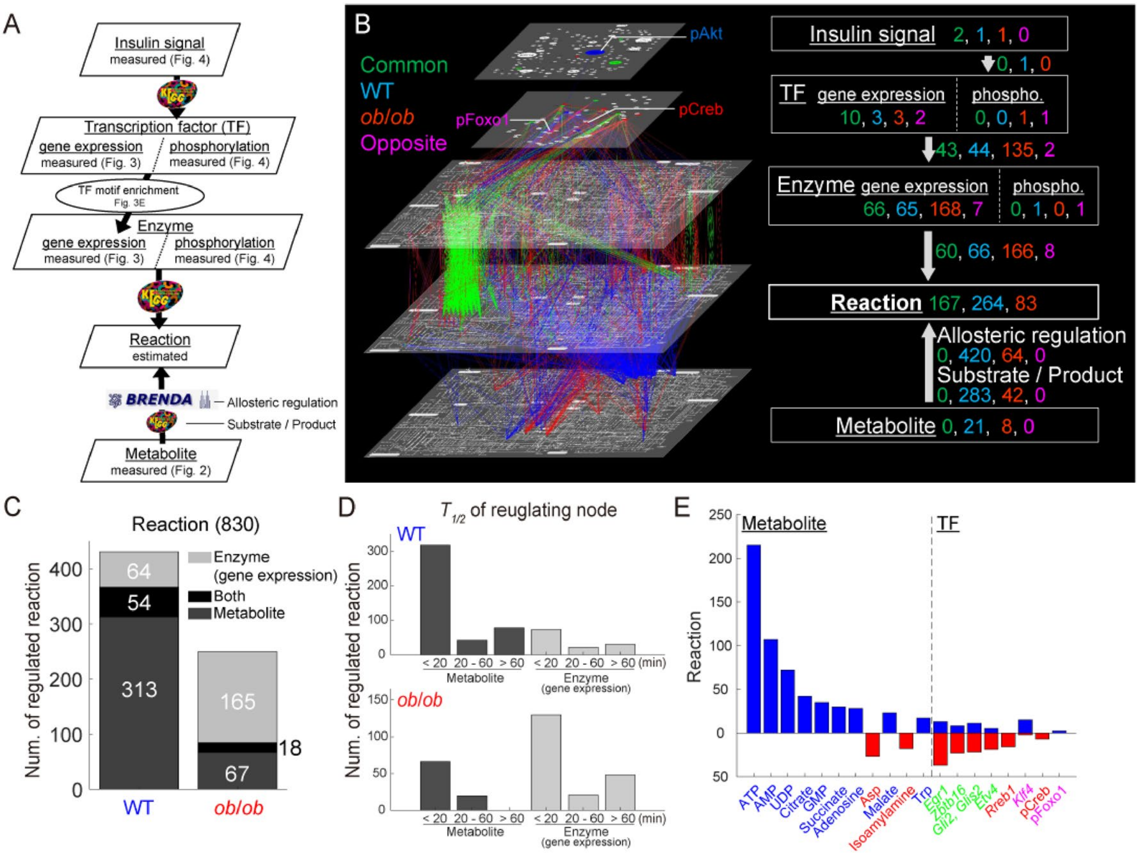

Figure 5. Construction of a regulatory transomic network for glucose-responsive metabolic reactions. (**A**) The procedure for constructing the regulatory transomic network for glucose-responsive metabolic reactions. The Insulin signal, TF, Enzyme, and Metabolite layers corresponded to glucose-responsive molecules. The Reaction layer represented "glucose-responsive metabolic reactions," which were defined as metabolic reactions regulated by glucose-responsive molecules. The arrows indicate interlayer regulatory connections. The databases used to identify the interlayer regulatory connections are shown by arrows. (**B**) The regulatory transomic network for glucose-responsive metabolic reactions. The left diagram represents the network as colored nodes in the layers and edges between the layers with colored nodes representing glucose-responsive molecules and colored edges representing interlayer regulatory connections: green, glucose-responsive molecules and interlayer regulation common in both WT and *ob*/*ob* mice; blue, specific to WT mice; red, specific to *ob*/*ob* mice; pink, opposite responses between WT and *ob*/*ob* mice. The numbers of each type of glucose-responsive node and edge are shown in the same colors in the network summary to the right. The Insulin signal layer was the insulin signaling pathway constructed in our previous phosphoproteomic study[11]. The Enzyme, Reaction, and Metabolite layers were organized into global metabolic pathways (mmu01100) in the KEGG database[18,19]. Phospho, phosphorylated. (**C**) The number of glucose-responsive metabolic reactions regulated by glucose-responsive molecules in the Enzyme layer, Metabolite layer, or both from a total of 830 metabolic reactions in the skeletal muscle. (**D**) The number of glucose-responsive metabolic reactions regulated by glucose-responsive metabolites and genes with the indicated time constants $T_{1/2}$ in WT mice (upper) and *ob*/*ob* mice (lower). (**E**) The number of glucose-responsive metabolic reactions regulated by the indicated glucose-responsive molecules in WT mice (upper, blue) and *ob*/*ob* mice (lower, red). The colors of the names of molecules indicate the type of glucose-responsive molecules as described in (**B**). Glucose-responsive metabolites and transcriptions factors that regulated more than 15 metabolic reactions are shown. The transcription factors encoded by glucose-responsive genes are italicized, and those showing glucose-responsive phosphorylation have the prefix "p."

for allosteric regulation. In this study, some amino acids including BCAA in the blood and skeletal muscle were decreased after glucose administration similar to the effect on the liver[12], suggesting suppression of protein degradation and promotion of protein synthesis in the insulin target organs[22,22,24,31]. In BCAA degradation pathway, as well as the decrease of the amino acids, we found the transcriptional repression of the metabolic enzymes, including *Bckdhb*, and the transcriptional activation of *Bckdk*, a inhibitory kinase of Bckdh[27], in *ob*/*ob* mice and partially in WT mice (Fig. 7C). These responses might suppress the degradation of BCAAs to the TCA cycle intermediates and contribute to the decrease in TCA cycle flux in the skeletal muscle. The blood level of a ketone body, an alternative energy source in the fasting state, was decreased in both WT and *ob*/*ob* mice after glucose administration. We also found that ketone levels in skeletal muscle showed a similar time series as those in the blood (Fig. 7D), suggesting that intramuscular degradation of ketone body to acetyl CoA was also reduced. Decreased degradation of these metabolites could contribute to a decrease in TCA cycle intermediates, but

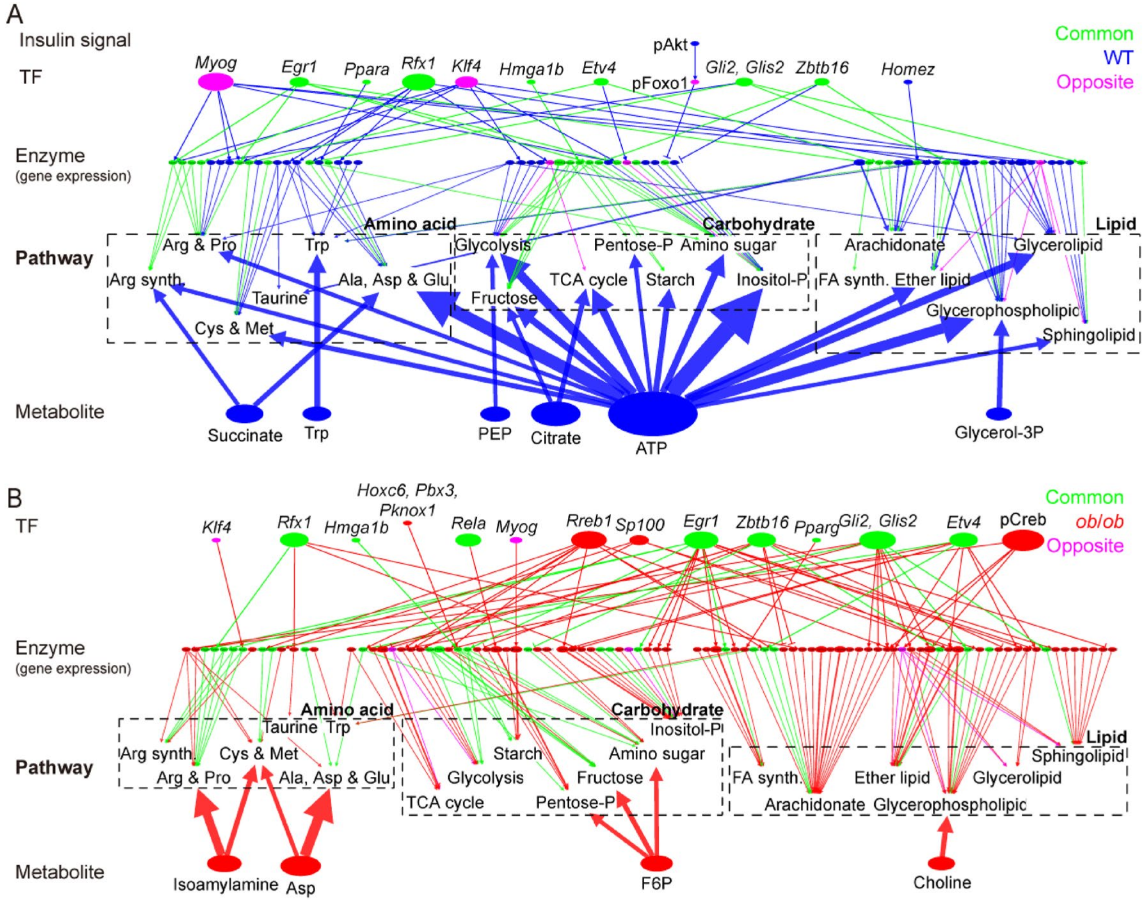
A
Insulin signal
TF
Enzyme
(gene expression)
Pathway
Metabolite
Common
WT
Opposite
pAkt
pFoxo1
Myog
Egr1
Ppara
Rfx1
Klf4
Hmga1b
Etv4
Gli2, Glis2
Zbtb16
Homez
Amino acid
Carbohydrate
Lipid
Arg & Pro
Trp
Arg synth.
Ala, Asp & Glu
Taurine
Cys & Met
Glycolysis
Pentose-P
Amino sugar
TCA cycle
Starch
Inositol-P
Fructose
Arachidonate
Glycerolipid
FA synth.
Ether lipid
Glycerophospholipid
Sphingolipid
Succinate
Trp
PEP
Citrate
ATP
Glycerol-3P
B
TF
Enzyme
(gene expression)
Pathway
Metabolite
Common
ob/ob
Opposite
Klf4
Rfx1
Hmga1b
Hoxc6, Pbx3, Pknox1
Rela
Myog
Rreb1
Sp100
Egr1
Zbtb16
Pparg
Gli2, Glis2
Etv4
pCreb
Amino acid
Carbohydrate
Lipid
Taurine
Trp
Arg synth.
Cys & Met
Arg & Pro
Ala, Asp & Glu
Starch
Inositol-P
Amino sugar
Glycolysis
Fructose
TCA cycle
Pentose-P
Sphingolipid
FA synth.
Ether lipid
Glycerolipid
Arachidonate
Glycerophospholipid
Isoamylamine
Asp
F6P
Choline

Figure 6. Condensed regulatory transomic networks for glucose-responsive metabolic reactions. (**A,B**) The condensed regulatory transomic network of the response to glucose in WT and *ob*/*ob* mice. The color of nodes (glucose-responsive molecules) and edges (interlayer regulatory connections) indicate the type of molecules and regulation as described in Fig. 5B. In the TF layer, the transcription factors encoded by glucose-responsive genes are italicized, and those showing glucose-responsive phosphorylation have the prefix "p." The Enzyme layer contained only the metabolic enzymes that were regulated by glucose-responsive changes in gene expression, and not those regulated only by phosphorylation. Two types of metabolic pathway nodes were included: the pathway that exhibited significant associations with any glucose-responsive molecule (Fig. S7B); and the pathway whose percentage of regulated reactions was in the top 10% by either glucose-responsive metabolites or by glucose-responsive genes encoding metabolic enzymes. Dashed boxes enclose the nodes for the lipid, carbohydrate, and amino acid classes. Glucose-responsive metabolites that exhibited significant associations with any metabolic pathway were included. Glucose-responsive transcription factors that regulated five or more metabolic reactions were included. The interlayer regulatory connections from the Metabolite to the Pathway layer included only those that regulate five or more metabolic reactions. The size of the nodes and width of the edges indicate the relative number of the regulated metabolic reactions. See Data File S10 for the unabbreviated names of the metabolic pathway nodes.

further research is needed to understand why the reduction was specific to WT mice. As mentioned above, the WT-specific responses of ATP, a product of the TCA cycle, and TCA cycle intermediates could activate glycolysis and glucose metabolism. Thus, elucidating the mechanism of the response will be helpful in understanding blood glucose homeostasis and its disruption by obesity.

We previously constructed a glucose-responsive transomic network in the liver of WT and *ob*/*ob* mice[12]. The liver network contained more glucose-responsive molecules and regulatory connections than the skeletal muscle network, but the differences between WT and *ob*/*ob* mice were similar between the liver and skeletal muscle. In both organs, many metabolic reactions in the WT networks were regulated by metabolites, whereas in the *ob*/*ob* networks, much of the regulation by metabolites was lost and metabolic regulation by gene expression was activated. There were also similarities in the regulation of the metabolic pathway, such as the regulation of carbohydrate metabolism by metabolites and the regulation of lipid metabolism by gene expression. We are currently performing a detailed comparative analysis between the liver network and skeletal muscle network.

To construct a comprehensive glucose-responsive network, it was necessary to integrate more omics data into our network. Because the Insulin signal layer was determined by western blot analysis, the numbers of glucose-responsive molecules and regulatory connections of the layer were very limited compared to those of the other layers. Integration of phosphoproteomic data and kinase-substrate interactions will facilitate a more extensive

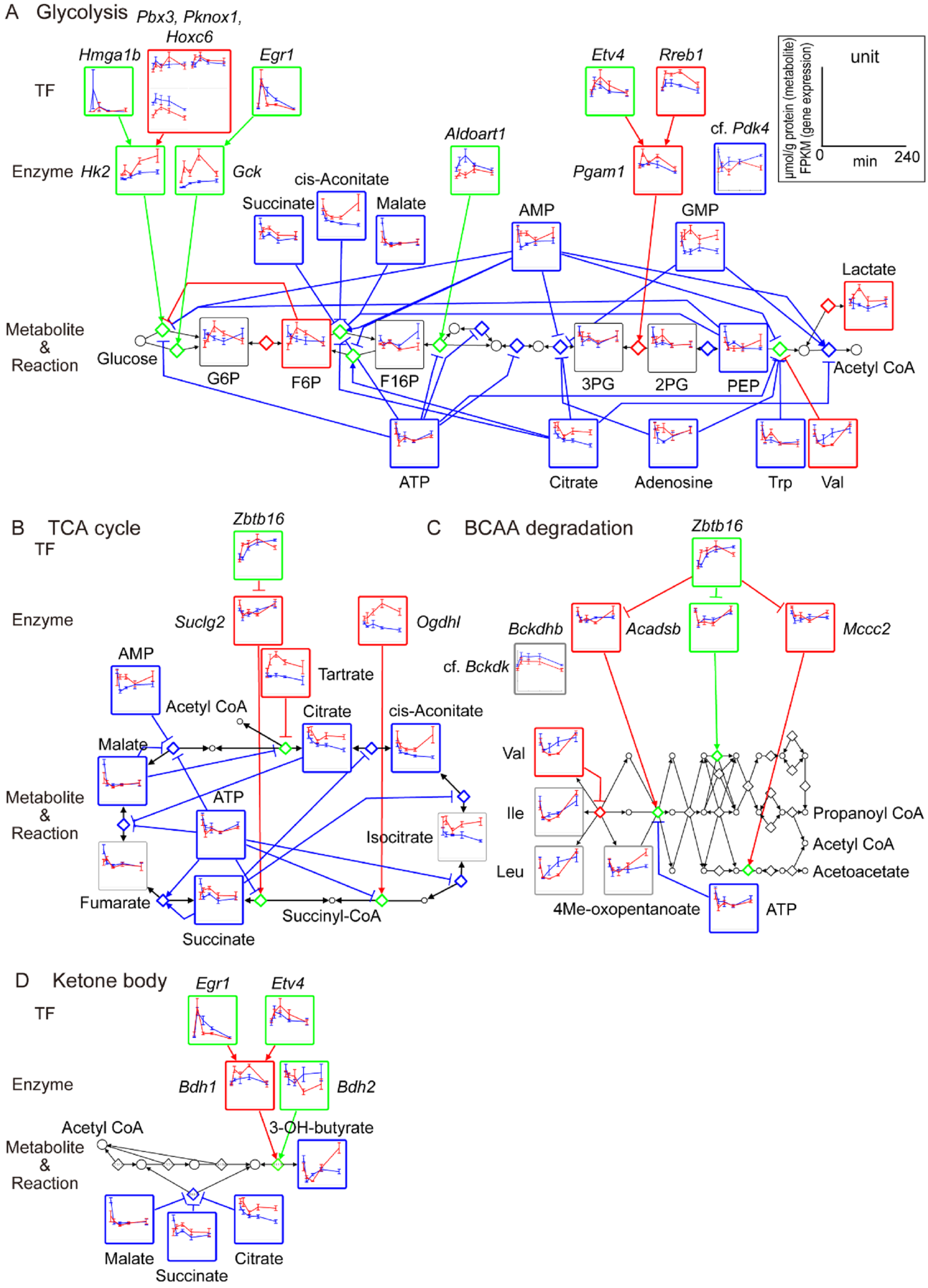
A Glycolysis
TF
Hmga1b
Pbx3, Pknox1, Hoxc6
Egr1
Etv4
Rreb1
unit
μmol/g protein (metabolite)
FPKM (gene expression)
0
min
240
Enzyme
Hk2
Gck
Aldoart1
Pgam1
cf. Pdk4
cis-Aconitate
Succinate
Malate
AMP
GMP
Lactate
Metabolite & Reaction
Glucose
G6P
F6P
F16P
3PG
2PG
PEP
Acetyl CoA
ATP
Citrate
Adenosine
Trp
Val
B TCA cycle
TF
Zbtb16
Enzyme
Suclg2
Ogdhl
AMP
Tartrate
Acetyl CoA
Citrate
cis-Aconitate
Malate
Metabolite & Reaction
ATP
Isocitrate
Fumarate
Succinate
Succinyl-CoA
C BCAA degradation
Zbtb16
Bckdhb
Acadsb
Mccc2
cf. Bckdk
Val
Ile
Leu
Propanoyl CoA
Acetyl CoA
Acetoacetate
4Me-oxopentanoate
ATP
D Ketone body
TF
Egr1
Etv4
Enzyme
Bdh1
Bdh2
Acetyl CoA
3-OH-butyrate
Metabolite & Reaction
Malate
Succinate
Citrate

◂**Figure 7.** Regulatory transomic network for glucose-responsive metabolic reactions in glycolysis, TCA cycle, BCAA degradation, and ketone body metabolism. The regulatory transomic network for glucose-responsive metabolic reactions in glycolysis (**A**), TCA cycle (**B**), BCAA degradation (**C**), and ketone body metabolism (**D**) in the skeletal muscle of WT mice and *ob*/*ob* mice. The information for the pathways was obtained from "glycolysis/gluconeogenesis" (mmu00010), "citrate cycle (TCA cycle)" (mmu00020), "valine, leucine and isoleucine degradation" (mmu00280), and "synthesis and degradation of ketone bodies" (mmu00072) in the KEGG database[18,19]. Graphs of the time courses of measured molecules are shown for corresponding nodes as the means and SEMs (n = 5 mice per genotype for metabolite, n = 11 or 12 mice per genotype for gene expression at 0 min, n = 5 mice per genotype for gene expression at 20, 60, 120, 240 min, n = 5 mice per genotype for phosphorylation). The colors of the frames indicate WT mice-specific glucose-responsive molecules (blue), *ob*/*ob* mice-specific glucose-responsive molecules (red), and common glucose-responsive molecules (green). The dashed frames indicate molecules that were not included in the glucose-responsive transomic network. Diamond nodes indicate metabolic reactions. The colored edges indicate interlayer regulatory connections: WT mice-specific regulatory connections (blue), *ob*/*ob* mice-specific regulatory connections (red), and common interlayer regulatory connections (green). From the Metabolite to Reaction layers, only allosteric regulatory connections are colored. Black edges indicate the relationship between metabolic reactions and its substrate/product. The reversibility of metabolic reactions was obtained from the KEGG database[18,19].

evaluation of the effects from the Insulin signal layer to the Reaction layer[32–34]. The transcription factors of the glucose-responsive genes were determined based on the binding motifs in the promoter sequences and the temporal patterns. Because not all motifs are bound by transcription factors, direct measurements of transcription factor binding using ChIP sequencing analysis will identify a more accurate and extensive regulatory network of glucose-responsive genes[17,35,36]. Furthermore, to accurately identify the effects of obesity on the glucose-responsive network, it is necessary to compare the glucose-responsive networks from various mouse models of obesity, such as HFD mice, as well as *ob*/*ob* mice. Although our transomic network was not comprehensive, we revealed several important features of metabolic regulation in the skeletal muscle after glucose administration. An extension of this in vivo transomic analysis will lead to a better understanding of glucose homeostasis at the whole-body level and its dysregulation in obesity.

Materials and methods

Animals and sample preparation.

Animal experiments were performed as previously described[12]. C57BL/6J WT mice or *ob*/*ob* mice at ten weeks of age were purchased from Japan SLC Inc. (Shizuoka, Japan). The phenotypic data of the mice are summarized in Table S1. Animal experiments were approved by the animal ethics committee of The University of Tokyo and according to the ARRIVE guidelines and the University of Tokyo guidelines for the care and use of laboratory animals. After purchasing, the mice were housed 2–3 to a cage and fasted overnight at 23 °C (6 p.m. to 10 a.m.). Overnight-fasted mice were administered an oral glucose load of 2 g/kg body weight (41.8–47.8 mg for WT mice, 76.8–94.4 mg for *ob*/*ob* mice). To measure blood glucose and insulin levels, 15 μL blood was collected from the tail veins at 0, 2, 5, 10, 15, 20, 30, 45, 60, 90, 120, 180, and 240 min after glucose administration (n = 5). We used the blood glucose and insulin levels measured in our previous study[12] (Fig. S2). For the metabolome and transcriptome studies, mice were sacrificed at 0, 20, 60, 120, and 240 min after glucose administration, and the gastrocnemius muscle was excised. Muscle samples were frozen immediately in liquid nitrogen and homogenized with dry ice. The powdered samples were divided and used for metabolomics, lipidomics, transcriptomics, a glycogen assay, and western blotting.

Metabolomics.

Metabolomic analysis was performed as previously described[12]. Total metabolites and proteins were extracted from the skeletal muscle with methanol:chloroform:water (2.5:2.5:1) extraction. Approximately 40 mg of the skeletal muscle was suspended in 500 μL ice-cold methanol containing internal standards (20 μM L-methionine sulfone [Wako], 2-morpholinoethanesulfonic acid, monohydrate [Dojindo], and D-camphor-10-sulfonic acid [Wako]) for normalization of MS peak intensities across runs, followed by suspension in 500 μL chloroform, and finally in 200 μL water. After centrifugation at 4600×*g* for 15 min at 4 °C, the aqueous layer was filtered through a 5 kDa molecular weight cutoff filter (Millipore) to remove protein contamination. The filtrate (320 μL) was lyophilized and, prior to MS analysis, dissolved in 50 μL water containing reference compounds (200 μM each of trimesate [Wako] and 3-aminopyrrolidine [Sigma-Aldrich]). Proteins were precipitated by adding 800 μL ice-cold methanol to the interphase and organic layers and centrifuged at 12,000×g for 15 min at 4 °C. The pellet was washed with 1 mL ice-cold 80% (v/v) methanol and resuspended in 1 mL sample buffer containing 1% sodium dodecyl sulfate (SDS) and 50 mM Tris-Cl pH8.8, followed by sonication. The total protein concentration was determined by the bicinchoninic acid (BCA) assay and was used for the normalization of metabolite concentration among samples.

All CE–MS experiments were performed using the Agilent 1600 Capillary Electrophoresis system (Agilent Technologies), the G1603A Agilent CE-MS adapter kit, and the G1607A Agilent CE electrospray ionization (ESI)–MS sprayer kit. Briefly, to analyze the cationic compounds, a fused silica capillary (50 μm internal diameter [i.d.] × 100 cm) was used with 1 M formic acid as the electrolyte[37]. Methanol/water (50% v/v) containing 0.01 μM hexakis(2,2-difluoroethoxy)phosphazene was delivered as the sheath liquid at 10 μL/min. ESI-time-of-flight (TOF) MS was performed in the positive ion mode, and the capillary voltage was set to 4 kV. Automatic recalibration of each acquired spectrum was achieved using the masses of the reference standards ([^{13}C isotopic ion of a protonated methanol dimer (2 MeOH + H)]$^+$, *m*/*z* 66.0631 and [hexakis(2,2-difluoroethoxy)phosphazene + H]$^+$, *m*/*z* 622.0290). To identify the metabolites, the relative migration times of all peaks were calculated by normalization to the reference compound 3-aminopyrrolidine. The metabolites were identified by comparing their *m*/*z* values and relative migration times to the metabolite standards. Quantification was performed by comparing peak areas to calibration curves generated using internal standardization techniques with methionine sulfone. The other conditions were identical to those previously described[38]. To analyze anionic metabolites, a commercially available COSMO(+) (chemically coated with cationic polymer) capillary (50 μm i.d. × 105 cm) (Nacalai Tesque, Kyoto, Japan) was used with a 50 mM ammonium acetate solution (pH 8.5) as the electrolyte. Methanol/5 mM ammonium acetate (50% v/v) containing 0.01 μM hexakis(2,2-difluoroethoxy)phosphazene was delivered as the sheath liquid at 10 μL/min. ESI-TOF MS was performed in the negative ion mode, and the capillary voltage was set to 3.5 kV. For anion analysis, trimesate and D-camphor-10-sulfonic acid were used as the reference and internal standard, respectively. The other conditions were identical to those described previously[39]. Agilent MassHunter software (Agilent technologies) was used for data analysis[38–40].

We used the blood metabolome data obtained in our previous study[12].

Lipidomics. Lipidomic analysis was performed as previously described[13]. Lipidomic profiling of the skeletal muscle was performed by Metabolon, Inc. Lipids were extracted from samples with dichloromethane and methanol using the modified Bligh and Dyer procedure in the presence of internal standards, with the lower organic phase used for analysis. The extracts were concentrated under nitrogen and reconstituted in 0.25 mL dichloromethane:methanol (50:50) containing 10 mM ammonium acetate. The extracts were placed in vials for infusion–MS analyses, which were performed on the SelexION equipped Sciex 5500 QTRAP mass spectrometer using both the positive and negative ion modes. Each sample was subjected to two analyses, with ion mobility spectrometry–MS conditions optimized for lipid classes monitored in each analysis. The 5500 QTRAP was operated in the multiple reaction monitoring mode to monitor the transitions for more than 1,100 lipids from up to 14 lipid classes. Individual lipid species were quantified based on the ratio of the signal intensity for target compounds to the signal intensity for an assigned internal standard of known concentration. Fourteen lipid class concentrations were calculated from the sum of all molecular species within a class.

Glycogen assay. Glycogen content was determined as previously described with some modifications[41]. Approximately 20 mg of the skeletal muscle was digested with 1.2 mL of 30% (w/v) potassium hydroxide solution for 1 h at 95 °C and neutralized with 61.2 μL glacial acetic acid. The total protein concentration of the muscle digest was determined by the BCA assay and adjusted to 1 μg protein/μL. Glycogen was extracted from the digested skeletal muscle using Bligh and Dyer method to remove lipids[42]. The digested skeletal muscle (50 μL) was mixed with 120 μL ice-cold methanol, 50 μL chloroform, 10 μL of 1% (w/v) linear polyacrylamide, and 70 μL water. After incubation on ice for 30 min, the mixture was centrifuged at 12,000×*g* to remove the separated aqueous layer. The glycogen was precipitated by the addition of 200 μL methanol and centrifugation at 12,000×*g* for 30 min at 4 °C, washed with ice-cold 80% (v/v) methanol, and dried completely. Glycogen pellets were suspended in 20 μL of 0.1 mg/mL amyloglucosidase (Sigma-Aldrich) in 50 mM sodium acetate buffer and incubated for 2 h at 55 °C to digest the glycogen. The concentration of the glucose produced from the glycogen was determined using the Amplex Red Glucose/Glucose Oxidase Assay kit (Thermo Fisher Scientific), according to the manufacturer's instructions.

Transcriptomics. Transcriptomic analysis was performed as previously described[12]. Total RNA was extracted from the skeletal muscle using the RNeasy Mini Kit (QIAGEN) and QIAshredder (QIAGEN); the quantity was assessed using the Nanodrop (Thermo Fisher Scientific) and the quality was assessed using the 2100 Bioanalyzer (Agilent Technologies). cDNA libraries were prepared using the SureSelect strand-specific RNA library preparation kit (Agilent Technologies). The resulting cDNAs were subjected to 100 base paired-end sequencing on the Illumina HiSeq2500 Platform (Illumina)[43]. Sequences were aligned to the mouse reference genome obtained from the Ensembl database[44,45] (GRCm38/mm10, Ensembl release 97) using the STAR software package TopHat (v.2.5.3a)[46]. The RSEM tool (v.1.3.0) was used to assemble transcript models (Ensembl release 97) from aligned sequences and to estimate gene expression level[47]. Gene expression level was shown as fragments per kilobase of exon per million mapped fragments.

Western blot analysis. Total proteins were extracted from the skeletal muscle with methanol:chloroform:water (2.5:2.5:1). Ice-cold methanol was added to the skeletal muscle at a concentration of 100 mg/mL of the weight of the skeletal muscle, and the suspension (400 μL) was mixed with chloroform (400 μL) and water (160 μL), followed by centrifugation at 4600×*g* for 10 min at 4 °C. The aqueous and organic phases were removed and 800 μL ice-cold methanol was added to the interphase to precipitate proteins. The resulting pellet was suspended with 400 μL lysis buffer (10 mM Tris–HCl [pH 6.8] in 1% SDS) and incubated for 15 min at 65 °C, followed by sonication. The protein lysate was centrifuged at 12,000×*g* for 3 min at 4 °C to remove debris. The total protein concentration of the resulting supernatant was determined by the BCA assay. The following primary antibodies were purchased from Cell Signaling Technology: phosphorylated Erk1/2 (p-Erk1/2, Thr^{202}/Tyr^{204}; #9101), pCreb (Ser^{133}; #9198), pAkt (Ser^{473}; #9271), pS6 (Ser^{235}/Ser^{236}; #2211), pGsk3β (Ser^{9}; #9336), pGs (Ser^{641}; #3891), pFoxo1 (Ser^{256}; #9461), pp38 (Thr^{180}/Tyr^{182}; #9211), and pAmpkα (Thr^{172}; #2531); pGp (Ser^{15}) was made in house as previously described[41]. The proteins (10 μg) were resolved by SDS-PAGE, electrotransferred to nitrocellulose membranes, and incubated with the appropriate antibodies. Immunodetection was performed using the Immobilon Western Chemiluminescent HRP Substrate (Millipore) or SuperSignal West Pico PLUS Chemiluminescent Substrate (Thermo Fisher Scientific), and the Western blot signals were detected using a luminoimage analyzer (LAS-4000; Fujifilm) and quantified with ImageJ software.

Identification of glucose-responsive molecules. Glucose-responsive molecules were determined as previously described[12]. Molecules that were detected in less than half of the replicates in either WT or *ob*/*ob* mice at any time point after oral glucose administration were removed from the analysis. A molecule with a statistically significant change in response to oral glucose administration was defined as a glucose-responsive molecule according to the following criteria. The fold change of the mean amount at each time point over the mean amount at fasting state (0 min) was calculated for each molecule. The significance of change at each time point was tested by the two-tailed Welch's *t*-test for each metabolite and phosphorylation, and by the edgeR package (version 3.26.8) of the R language (version 3.6.1) with the default parameters for each gene[48]. Metabolite, gene, and phosphorylation that showed an absolute $\log_2$ fold change ≥ 0.585 ($2^{0.585} = 1.5$) and an FDR-adjusted p value (q value) ≤ 0.1 at any time point were defined as a glucose-responsive metabolite (Fig. 2A,B), gene (Fig. 3A,B), and phosphorylation (Fig. 4). The q values were calculated by Storey's procedure[49]. To define an increase or decrease in time courses with changes in both directions at different times, we used the direction of change compared to time 0 at the earliest time point that showed a significant change.

Clustering analysis. Time courses for each metabolite of WT mice and *ob*/*ob* mice were normalized by dividing by the geometric mean of the values of WT mice and *ob*/*ob* mice in the fasting state (0 min) followed by $\log_2$ transformation. We combined the two time courses of WT and *ob*/*ob* mice for each metabolite and performed hierarchical clustering of the combined time courses using Euclidean distance and Ward's method (Fig. S3). Based on the clustering tree, we defined eight different clusters of metabolites, showing similar or different responses between WT and *ob*/*ob* mice.

Clustering analysis of gene expression was performed as previously described with some modifications[12]. Time courses for the expression of each gene of WT and *ob*/*ob* mice were normalized by subtracting the average expression values of the time courses of both mice and then dividing the resulting values by the standard deviation (Z-score normalization). We combined the two time courses of WT and *ob*/*ob* mice for each gene and performed hierarchical clustering of the combined time courses using Euclidean distance and Ward's method (Fig. S7A). The genes with significant differences between WT and *ob*/*ob* mice before glucose administration (0 min) (q value < 0.1) or a significant response at any time point in either WT or *ob*/*ob* mice (q value < 0.1) were selected for the clustering analysis (12,301 genes). For the selection, the *p* value was calculated using the edgeR package (version 3.26.8) of the R language (version 3.6.1) with the default parameters[48], and the q value was calculated by Storey's procedure[49].

Pathway enrichment analysis. We performed pathway enrichment analysis of glucose-responsive genes (Table 1; Data File S4). The enrichment of the genes in each pathway was determined using the one-tailed Fisher's exact test. We used the genes detected in more than half of the replicates in WT and *ob*/*ob* mice at all time points as background. We used the pathways in Metabolism, Genetic Information Processing, and Cellular Processes from the KEGG database[18,19].

Prediction of the transcription factor binding motif and inference of regulatory connections between transcription factors and genes. Analysis of transcription factors was performed as previously described[12]. The flanking regions around the major transcription start site of genes were extracted from GRCm38/mm10 (Ensembl, release 97) using Ensembl BioMart[50]. The region from -300 bp to + 100 bp of the major transcription start site was defined as the flanking region, according to FANTOM5 analysis of the time course[51]. The transcription factor binding motifs in each flanking region (Fig. S5B) were predicted using TRANSFAC Pro, a transcription factor database, and Match, a transcription factor binding motif prediction tool[15,16]. The threshold for each transcription factor binding motif prediction was set using extended vertebrate_non_redundant_min_FP.prf, a parameter set in TRANSFAC Pro[12].

For the inference of regulatory connections between transcription factors and genes, we performed transcription factor motif enrichment analysis of the genes in each cluster (Fig. S5B). The enrichment of transcription factor binding motif in the flanking regions of genes in each cluster was determined by the one-tailed Fisher's exact test, and transcription factor binding motifs with q value ≤ 0.1 were defined as significantly enriched. The q values were calculated by the Benjamini–Hochberg procedure[52]. We used the genes analyzed in the hierarchical clustering as background. To reduce the number of statistical tests, the clusters that contained ≥ 100 genes were analyzed. If a transcription factor binding motif was enriched in the promoter regions of the genes in a cluster, we inferred the regulatory connections between the corresponding transcription factor and the genes in the cluster. To avoid overestimation, we excluded a cluster from the inference if the transcription factor binding motif was more enriched in the children clusters that contained ≥ 100 genes. To compare the enrichment of transcription factor binding motifs between clusters, we calculated the odds ratio of the transcription factor binding motifs for each cluster.

For validation of the inferred regulatory connections, we examined the overlap between the inferred genes of each transcription factor and those predicted from experimental ChIP data from the ChIP-Atlas database[17] (Fig. S5C). The genes for which ChIP sequencing peaks of a transcription factor were detected in the flanking region around the transcription start sites were obtained using "Target Genes," a prediction tool in the ChIP-Atlas. We used the flanking regions from − 1000 to + 1000 bp of the transcription start sites in Target Genes. The overlap between the inferred genes and genes from ChIP data was determined by the one-tailed Fisher's exact test, and those with q value ≤ 0.1 were defined as significant. The q values were calculated by the Benjamini–Hochberg procedure[52].

Insulin signaling pathway. The insulin signaling pathway in Fig. 4 is a subset of the nodes of the insulin signaling pathway in the KEGG database (mmu04910)[18,19]. We added regulatory input to Creb from the PI3K-Akt signaling pathway (mmu04151), MAPK signaling pathway (mmu04010), and AMPK signaling pathway (mmu04152), and regulatory input to FoxO1 from the FoxO signaling pathway (mmu04068) in the KEGG database. The edges from Akt to Ampk and from p38 to insulin receptor substrate were added according to previous studies[53,54].

Construction of the regulatory glucose-responsive transomic network. The transomic network was constructed as previously described with some modifications[12]. The regulatory glucose-responsive transomic networks consisted of five layers, namely Insulin signal, TF, Enzyme, Reaction, and Metabolite, with interlayer regulatory connections (Fig. 5A,B). The Insulin signal layer is the insulin signaling pathway constructed in our previous phosphoproteomic study[11]. We included in the Insulin signal layer signaling molecules that we analyzed by western blotting; we did not include transcription factors such as Foxo1, or metabolic enzymes such as Gs in this layer. The TF layer consisted of all transcription factors with an inferred regulatory connection (Fig. S7B). The Enzyme layer consisted of all metabolic enzymes in the pathways in Metabolism obtained from the KEGG database[18,19]. The Reaction layer consisted of the metabolic reactions (based on EC number) corresponding to the metabolic enzymes in the Enzyme layer. The Metabolite layer consisted of all metabolites analyzed by CE–MS. Only the molecules and reactions corresponding to genes that were expressed in at least one sample were included in the Insulin signal, TF, Enzyme, and Reaction layers. Not all 15,608 genes were included in the network.

Glucose-responsive molecules were assigned to the corresponding layers as nodes. The Insulin signal layer consisted of insulin signaling molecules with glucose-responsive phosphorylation. The TF layer consisted of transcription factors encoded by glucose-responsive genes or those with glucose-responsive phosphorylation. The Enzyme layer consisted of metabolic enzymes encoded by glucose-responsive genes or those with glucose-responsive phosphorylation. The Reaction layer consisted of "glucose-responsive metabolic reactions," which were defined as metabolic reactions regulated by glucose-responsive molecules. The Metabolite layer consisted of glucose-responsive metabolites. We also determined the direction of glucose responsiveness. To determine a direction for time courses with both increased and decreased time points, we used the direction of change at the earliest time point with a significant difference from time 0 (fasting state). We did not determine a direction (increase or decrease) for metabolic reactions because we did not measure metabolic reaction activity.

To determine regulatory connections from the Enzyme and Metabolite layers to the Reaction layer, both the target of the regulatory connection (a metabolic reaction) and the regulating molecule (enzyme or metabolite) had to be glucose-responsive. Among the Insulin signal, TF, and Enzyme layers, the interlayer regulatory connections were determined using the directions of glucose responsiveness of the regulating molecule and the regulated molecules, and the types of interlayer regulatory connections, which were designated as either positive or negative. We defined positive interlayer regulatory connections as when both the regulating molecule and regulated molecule showed the same direction of change, namely, both increased or both decreased. We defined negative interlayer regulatory connections as when the regulating molecule and regulated molecule showed responses in the opposite direction, namely, one increased and the other decreased.

The interlayer regulatory connections between glucose-responsive molecules were determined according to databases. The interlayer connections from the Insulin signal layer to the TF layer were determined by the regulation of transcription factors by kinases retrieved from the KEGG database[18,19]. The interlayer connections from the TF layer to the Enzyme layer were determined from inferred regulatory connections between transcription factors and genes (Fig. 3E). The interlayer connections from the Enzyme layer to the Reaction layer were determined by connecting metabolic reactions to their corresponding metabolic enzymes according to the KEGG database[18,19]. The interlayer connections from the Metabolite layer to the Reaction layer comprised two types of regulatory connections: those mediated by allosteric regulators, which were retrieved from the BRENDA database[20], and those mediated by the substrate or product of the reaction, which were retrieved from the KEGG database[18,19]. The types of regulatory connections made by glucose-responsive transcription factors were defined according to the Gene Ontology (GO) annotations obtained from the Mouse Genome Database[55] (Data File S6). The transcription factors that were included in the list of DNA-binding transcription repressors (GO:0001227) and not in the list of DNA-binding transcription activators (GO:0001228) were defined as transcription repressors. Foxo1 was added to the list of transcription activators based on previous studies of gluconeogenesis[56,57]. The effects of the phosphorylation of transcription factors on the types of regulatory connections were defined according to the KEGG database[18,19]. We used the allosteric regulation reported for mammals (*Bos taurus*, *Felis catus*, *Homo sapiens*, "Macaca," "Mammalia," "Monkey," *Mus booduga*, *Mus musculus*, *Rattus norvegicus*, *Rattus rattus*, *Rattus sp*., *Sus scrofa*, "dolphin," and "hamster") according to the BRENDA database[20]. Because the reversibility of metabolic reactions was not determined, metabolic reactions were assumed to be regulated by both the substrate and product.

Generation of a condensed transomic network based on metabolic pathway information. We condensed the regulatory transomic networks as previously described with some modifications[12]. First, we grouped the related metabolic reactions in a specific metabolic pathway into one "metabolic pathway node" (Pathway layer), and classified the metabolic pathway nodes into three classes—carbohydrate, lipid, and amino acid—according to the KEGG database[18,19]. Second, we selected two types of metabolic pathway nodes: one was a pathway that exhibited significant associations with any glucose-responsive metabolites or transcription factors; the other was a pathway whose percentage of regulated reactions was in the top 10% either by glucose-responsive metabolites or by glucose-responsive genes encoding metabolic enzymes (Fig. S7A). The association between the metabolic reactions in a metabolic pathway and those regulated by a glucose-responsive molecule was determined by the one-tailed Fisher's exact test, and associations with a q value ≤ 0.01 were defined as significant. The q values were calculated by the Benjamini–Hochberg procedure[52]. We also selected glucose-responsive metabolites that exhibited significant associations with any metabolic pathway nodes and glucose-responsive transcription factors that regulate five or more metabolic enzymes. Third, we reduced the interlayer regulatory connections from the Metabolite layer to the Pathway layer by removing the interlayer regulatory connections that regulated fewer than five metabolic reactions.

Implementation. Statistical tests, clustering analysis, enrichment analysis, and transomic network analysis were done using MATLAB 2020a (The Mathworks Inc.). Visualization of transomic network in the Graph Modeling Language formats was done using Python 2.7 and VANTED[58].

Data availability

Sequencing data measured in this study have been deposited in the DNA Data Bank of Japan Sequence Read Archive (DRA) (www.ddbj.nig.ac.jp/) under the accession no. DRA008416. All other data needed to evaluate the conclusions in the paper are present in the paper or Supplementary Materials. The code used for the analysis in this paper is available upon request.

Received: 13 May 2022; Accepted: 3 August 2022
Published online: 12 August 2022

References

1. Evans, R. M., Barish, G. D. & Wang, Y. X. PPARs and the complex journey to obesity. *Nat. Med.* **10**, 355–361 (2004).
2. Kahn, S. E., Hull, R. L. & Utzschneider, K. M. Mechanisms linking obesity to insulin resistance and type 2 diabetes. *Nature* **444**, 840–846 (2006).
3. DeFronzo, R. A. & Tripathy, D. Skeletal muscle insulin resistance is the primary defect in type 2 diabetes. *Diabetes Care* **32**(Suppl 2), S157–S163 (2009).
4. Hasin, Y., Seldin, M. & Lusis, A. Multi-omics approaches to disease. *Genome Biol.* **18**, 1–15 (2017).
5. Wiley, H. S. Integrating multiple types of data for signaling research: Challenges and opportunities. *Sci. Signal.* **4**, 1–4 (2011).
6. Soltis, A. R. *et al.* Hepatic dysfunction caused by consumption of a high-fat diet. *Cell Rep.* **21**, 3317–3328 (2017).
7. Piening, B. D. *et al.* Integrative personal omics profiles during periods of weight gain and loss. *Cell Syst.* https://doi.org/10.1016/j.cels.2017.12.013 (2018).
8. Yugi, K. *et al.* Reconstruction of insulin signal flow from phosphoproteome and metabolome data. *Cell Rep.* **8**, 1171–1183 (2014).
9. Yugi, K., Kubota, H., Hatano, A. & Kuroda, S. Trans-omics: How to reconstruct biochemical networks across multiple 'omic' layers. *Trends Biotechnol.* **34**, 276–290 (2016).
10. Yugi, K. & Kuroda, S. Metabolism as a signal generator across trans-omic networks at distinct time scales. *Curr. Opin. Syst. Biol.* **8**, 59–66 (2018).
11. Kawata, K. *et al.* Trans-omic analysis reveals selective responses to induced and basal insulin across signaling, transcriptional, and metabolic networks. *iScience* **7**, 212–229 (2018).
12. Kokaji, T. *et al.* Transomics analysis reveals allosteric and gene regulation axes for altered hepatic glucose-responsive metabolism in obesity. *Sci. Signal.* **13**, 660 (2020).
13. Egami, R. *et al.* Trans-omic analysis reveals obesity-associated dysregulation of inter-organ metabolic cycles between the liver and skeletal muscle. *iScience* **24**, 102217 (2021).
14. Katz, J. & Tayek, J. A. Gluconeogenesis and the Cori cycle in 12-, 20-, and 40-h-fasted humans. *Am. J. Physiol.* **275**, E537–E542 (1998).
15. Matys, V. *et al.* TRANSFAC(R) and its module TRANSCompel(R): transcriptional gene regulation in eukaryotes. *Nucl. Acids Res.* **34**, D108-110 (2006).
16. Kel, A. E. *et al.* MATCH™: A tool for searching transcription factor binding sites in DNA sequences. *Nucleic Acids Res.* **31**, 3576–3579 (2003).
17. Oki, S. *et al.* ChIP-Atlas: A data-mining suite powered by full integration of public ChIP-seq data. *EMBO Rep.* **19**, e46255 (2018).
18. Kanehisa, M., Goto, S., Sato, Y., Furumichi, M. & Tanabe, M. KEGG for integration and interpretation of large-scale molecular data sets. *Nucleic Acids Res.* **40**, D109–D114 (2012).
19. Kanehisa, M., Furumichi, M., Tanabe, M., Sato, Y. & Morishima, K. KEGG: New perspectives on genomes, pathways, diseases and drugs. *Nucleic Acids Res.* **45**, D353–D361 (2017).
20. Schomburg, I. *et al.* BRENDA in 2013: Integrated reactions, kinetic data, enzyme function data, improved disease classification: New options and contents in BRENDA. *Nucleic Acids Res.* **41**, 764–772 (2013).
21. Furuyama, T., Kitayama, K., Yamashita, H. & Mori, N. Forkhead transcription factor F0X01 (FKHR)-dependent induction of PDK4 gene expression in skeletal muscle during energy deprivation. *Biochem. J.* **375**, 365–371 (2003).
22. Dimitriadis, G., Mitron, P., Lambadiari, V., Maratou, E. & Raptis, S. A. Insulin effects in muscle and adipose tissue. *Diabetes Res. Clin. Pract.* **93**, 52–59 (2011).
23. Puchalska, P. & Crawford, P. A. Multi-dimensional roles of ketone bodies in fuel metabolism, signaling, and therapeutics. *Cell Metab.* **25**, 262–284 (2017).
24. Saxton, R. A. & Sabatini, D. M. mTOR signaling in growth, metabolism, and disease. *Cell* **168**, 960–976 (2017).
25. Koves, T. R. *et al.* Mitochondrial overload and incomplete fatty acid oxidation contribute to skeletal muscle insulin resistance. *Cell Metab.* **7**, 45–56 (2008).
26. Wong, K. E. *et al.* Muscle-specific overexpression of PGC-1α does not augment metabolic improvements in response to exercise and caloric restriction. *Diabetes* **64**, 1532–1543 (2015).
27. Lynch, C. J. & Adams, S. H. Branched-chain amino acids in metabolic signalling and insulin resistance. *Nat. Rev. Endocrinol.* **10**, 723–736 (2014).
28. Lopes, M. *et al.* Metabolomics atlas of oral 13C-glucose tolerance test in mice. *Cell Rep.* **37**, 109833 (2021).
29. Brooks, G. A. Lactate as a fulcrum of metabolism. *Redox Biol.* **35**, 101454 (2020).
30. Hui, S. *et al.* Quantitative fluxomics of circulating metabolites. *Cell Metab.* **32**, 676-688.e4 (2020).
31. Ruvinsky, I. & Meyuhas, O. Ribosomal protein S6 phosphorylation: From protein synthesis to cell size. *Trends Biochem. Sci.* **31**, 342–348 (2006).
32. Humphrey, S. J. *et al.* Dynamic adipocyte phosphoproteome reveals that Akt directly regulates mTORC2. *Cell Metab.* **17**, 1009–1020 (2013).

33. Krycer, J. R. *et al.* Dynamic metabolomics reveals that insulin primes the adipocyte for glucose metabolism. *Cell Rep.* **21**, 3536–3547 (2017).
34. Ohno, S. *et al.* Kinetic trans-omic analysis reveals key regulatory mechanisms for insulin-regulated glucose metabolism in adipocytes. *iScience* **23**, 101479 (2020).
35. Chèneby, J., Gheorghe, M., Artufel, M., Mathelier, A. & Ballester, B. ReMap 2018: An updated atlas of regulatory regions from an integrative analysis of DNA-binding ChIP-seq experiments. *Nucleic Acids Res.* **46**, D267–D275 (2018).
36. Yevshin, I., Sharipov, R., Kolmykov, S., Kondrakhin, Y. & Kolpakov, F. GTRD: A database on gene transcription regulation—2019 update. *Nucleic Acids Res.* **47**, D100–D105 (2019).
37. Soga, T. & Heiger, D. N. Amino acid analysis by capillary electrophoresis electrospray ionization mass spectrometry. *Anal. Chem.* **72**, 1236–1241 (2000).
38. Soga, T. *et al.* Differential metabolomics reveals ophthalmic acid as an oxidative stress biomarker indicating hepatic glutathione consumption. *J. Biol. Chem.* **281**, 16768–16776 (2006).
39. Soga, T. *et al.* Metabolomic profiling of anionic metabolites by capillary electrophoresis mass spectrometry. *Anal. Chem.* **81**, 6165–6174 (2009).
40. Ishii, N. *et al.* Multiple high-throughput analyses monitor the response of *E. coli* to perturbations. *Science* **316**, 593–597 (2007).
41. Noguchi, R. *et al.* The selective control of glycolysis, gluconeogenesis and glycogenesis by temporal insulin patterns. *Mol. Syst. Biol.* **9**, 664 (2013).
42. Von Wilamowitz-Moellendorff, A. *et al.* Glucose-6-phosphate-mediated activation of liver glycogen synthase plays a key role in hepatic glycogen synthesis. *Diabetes* **62**, 4070–4082 (2013).
43. Matsumoto, K., Suzuki, A., Wakaguri, H., Sugano, S. & Suzuki, Y. Construction of mate pair full-length cDNAs libraries and characterization of transcriptional start sites and termination sites. *Nucleic Acids Res.* **42**, e125 (2014).
44. Flicek, P. *et al.* Ensembl 2014. *Nucleic Acids Res.* **42**, 749–755 (2014).
45. Cunningham, F. *et al.* Ensembl 2015. *Nucleic Acids Res.* **43**, D662–D669 (2015).
46. Dobin, A. *et al.* STAR: Ultrafast universal RNA-seq aligner. *Bioinformatics* **29**, 15–21 (2013).
47. Li, B. & Dewey, C. N. RSEM: accurate transcript quantification from RNA-Seq data with or without a reference genome. *BMC Bioinform.* **12**, 323 (2011).
48. Robinson, M. D., McCarthy, D. J. & Smyth, G. K. edgeR: A Bioconductor package for differential expression analysis of digital gene expression data. *Bioinformatics* **26**, 139–140 (2009).
49. Storey, J. D. A direct approach to false discovery rates. *J. R. Stat. Soc. Ser. B Stat. Methodol.* **64**, 479–488 (2002).
50. Kinsella, R. J. *et al.* Ensembl BioMarts: A hub for data retrieval across taxonomic space. *Database* **2011**, 1–9 (2011).
51. Arner, E. *et al.* Transcribed enhancers lead waves of coordinated transcription in transitioning mammalian cells. *Science* **347**, 1010–1014 (2015).
52. Yoav Benjamini, Y. H. Controlling the false discovery rate : A practical and powerful approach to multiple testing. *J. R. Stat. Soc.* **57**, 289–300 (1995).
53. Jaiswal, N. *et al.* The role of skeletal muscle Akt in the regulation of muscle mass and glucose homeostasis. *Mol. Metab.* **28**, 1–13 (2019).
54. Archuleta, T. L. *et al.* Oxidant stress-induced loss of IRS-1 and IRS-2 proteins in rat skeletal muscle: Role of p38 MAPK. *Free Radic. Biol. Med.* **47**, 1486–1493 (2009).
55. Bult, C. J. *et al.* The Mouse Genome Database (MGD): Mouse biology and model systems. *Nucleic Acids Res.* **36**, D724–D728 (2008).
56. Barthel, A., Schmoll, D. & Unterman, T. G. FoxO proteins in insulin action and metabolism. *Trends Endocrinol. Metab.* **16**, 183–189 (2005).
57. Nakae, J., Kitamura, T., Silver, D. L. & Accili, D. The forkhead transcription factor Foxo1 (Fkhr) confers insulin sensitivity onto glucose-6- phosphatase expression. *J. Clin. Investig.* **108**, 1359–1367 (2001).
58. Junker, B. H., Klukas, C. & Schreiber, F. Vanted: A system for advanced data analysis and visualization in the context of biological networks. *BMC Bioinform.* **7**, 1–13 (2006).

Acknowledgements

We thank Maki Ohishi, Ayano Ueno, Hiroko Maki, Keiko Endo, and Sanae Ashitani (Keio University) for their technical assistance with metabolomic analysis using CE–MS; and our laboratory members for critically reading this manuscript and for their technical assistance with the experiments. The computational analysis of this work was performed in part with support of the super computer system of the National Institute of Genetics (NIG), Research Organization of Information and Systems (ROIS).

Author contributions

T.K., M.E., A.H., K.M., Y.I., R.E., and H.K. designed and performed the animal experiments, enzyme assays and western blot analysis. A.H. and T.S. performed metabolomic analysis using CE–MS. Y.S. performed RNA sequencing transcriptomic analysis. T.K., K.Y., S.O., M.F., K.H., Y.I., S.U., A.T., Y.P., H.M., D.L., Y.B., T.T., and H.O. performed transomic analysis. The writing group consisted of T.K., M.E., H.I., and S.K. The study was conceived and supervised by T.K. and S.K.

Funding

This work was supported by CREST (JPMJCR2123) from the Japan Science and Technology Agency (JST) and by the Japan Society for the Promotion of Science (JSPS) KAKENHI Grant Number JP17H06300, JP17H06299, JP18H03979. T.K. receives funding from a Grant-in-Aid for Early-Career Scientists (JP21K16349). K.Y. receives funding from JSPS KAKENHI Grant Number JP15H05582, JP18H05431, and “Creation of Innovative Technology for Medical Applications Based on the Global Analyses and Regulation of Disease- Related Metabolites”, PRESTO (JPMJPR1538) from JST. K.M. receives funding from a Grant-in-Aid for Early-Career Scientists (JP21K15342). S.O. receives funding from a Grant-in-Aid for Young Scientists (B) (JP17K14864, JP21K14467). M.F. receives funding from a Grant-in-Aid for Challenging Exploratory Research (JP16K12508). T.T. was supported by JSPS KAKENHI Grant Number JP19K24361, JP20K19915. H.O. was supported by JSPS KAKENHI Grant Number JP19H03696, JP19K20394. H. I. was supported by JSPS KAKENHI Grant Number JP18KT0020, JP17H05499, and by Adaptable and Seamless Technology transfer Program through Target-driven R&D (A-STEP) from JST. H.K. was supported by JSPS KAKENHI Grant Number JP20H03237. Y.S. was supported by the JSPS KAKENHI Grant Number JP17H06306. A. Hirayama was supported by the JSPS KAKENHI Grant Number JP18H04804.

T.S. receives funding from the AMED-CREST from the Japan Agency for Medical Research and Development (AMED) under Grant Number JP18gm0710003.

Competing interests

The authors declare no competing interests.

Additional information

Supplementary Information The online version contains supplementary material available at https://doi.org/10.1038/s41598-022-17964-9.

Correspondence and requests for materials should be addressed to S.K.

Reprints and permissions information is available at www.nature.com/reprints.

Publisher's note Springer Nature remains neutral with regard to jurisdictional claims in published maps and institutional affiliations.

Open Access This article is licensed under a Creative Commons Attribution 4.0 International License, which permits use, sharing, adaptation, distribution and reproduction in any medium or format, as long as you give appropriate credit to the original author(s) and the source, provide a link to the Creative Commons licence, and indicate if changes were made. The images or other third party material in this article are included in the article's Creative Commons licence, unless indicated otherwise in a credit line to the material. If material is not included in the article's Creative Commons licence and your intended use is not permitted by statutory regulation or exceeds the permitted use, you will need to obtain permission directly from the copyright holder. To view a copy of this licence, visit http://creativecommons.org/licenses/by/4.0/.

© The Author(s) 2022